THE REFLECTIVITY OF NEUTRONS BY DISTORTED COPPER CRYSTALS

THE REFLECTIVITY OF NEUTRONS BY DISTORTED COPPER CRYSTALS

by

RONALD ROY DYMOND, B.Sc.

A Thesis

Submitted to the Faculty of Graduate Studies

in Partial Fulfilment of the Requirements

for the Degree

Master of Science

McMaster University

September 1970

MASTER OF SCIENCE (1970) MCMASTER UNIVERSITY
(Physics) Hamilton, Ontario

TITLE: The Reflectivity of Neutrons by Distorted Copper Crystals.

AUTHOR: Ronald Roy Dymond, B.Sc. (University of Western Ontario)

SUPERVISOR: Professor B. N. Brockhouse, F.R.S.

NUMBER OF PAGES: x, 86

SCOPE AND CONTENTS:

The wavelength dependence of the integrated and peak reflectivities of distorted copper single crystals has been measured and the results compared with calculated values obtained from Bacon and Lowde's model of an ideally imperfect mosaic crystal. The effects of simultaneous reflections on the reflected neutron intensities were studied and accounted for in terms of an effective absorption coefficient. A non-Gaussian mosaic block distribution function was successfully introduced to bring about better agreement between experimental and calculated curve shapes. Using this technique, the desired agreement in curve shape was attained but, in order to bring measured and calculated absolute reflectivities into better agreement, it was necessary to include primary extinction effects.

ACKNOWLEDGEMENTS

I would like to thank the National Research Council of Canada for their financial support in the form of a National Research Council Scholarship. I would also like to thank the Atomic Energy of Canada Ltd. for use of their facilities at the Chalk River Nuclear Laboratories.

To my collegues in the neutron and solid state physics group at McMaster University; Mr. J.R.D. Copley, Mr. D.H. Dutton, Mr. W.A. Kamitakahara, Mr. A. Larose, Mr. A.P. Roy, and Mr. H.C. Teh, go my sincere thanks for their assistance in my experiments and for their friendship over the past two years.

I would especially like to thank Dr. E.D. Hallman who initiated the work on copper crystal monochromators here at McMaster. His guidance and patience in initiating me into this work is greatly appreciated.

Most of all, I would like to thank my research supervisor, Dr. B.N. Brockhouse, F.R.S., for his continuing guidance and many helpful discussions. His constant enthusiasm for the field of solid state physics has been a true inspiration.

Thanks are also due to Mrs. S. McQueen for her cooperation in typing a major portion of this thesis, and to Mrs. S. Duke and Mr. J. Ho for the drawing of all the figures found within it.

TABLE OF CONTENTS

LIST OF FIGURES

LIST OF TABLES

CHAPTER I

INTRODUCTION

The usefulness of neutron spectrometry in the study of the properties of solids and liquids has demanded an ever increasing source of neutrons as the complexity of experiments becomes more and more involved. The neutron source is, of course, a nuclear reactor. The flux of neutrons from such a reactor follows, approximately, a Maxwellian spectrum (Fig. I-1) described by

$$n(E)dE = \frac{E}{(k_B T)^2} \exp\left(\frac{-E}{k_B T}\right) dE \qquad \text{I-1}$$

where $n(E)dE$ = the flux of neutrons with energy between E and E + dE.

The purpose of the neutron monochromator is to select out neutrons of desired energy from the spectrum described above, thus providing access to a beam of monochromatic neutrons which can be used in various experiments. This selection process must be as efficient as possible since the fluxes available from nuclear reactors are very low ($\sim 10^{15}$ neutrons/cm^2-sec) compared, for example, with fluxes available for X-ray or optical studies. Thus, the efficiency of the monochromator system is of paramount importance, especially when working at the extreme ends of the reactor spectrum where the neutron flux is very low.

There are two fundamental types of monochromators in use

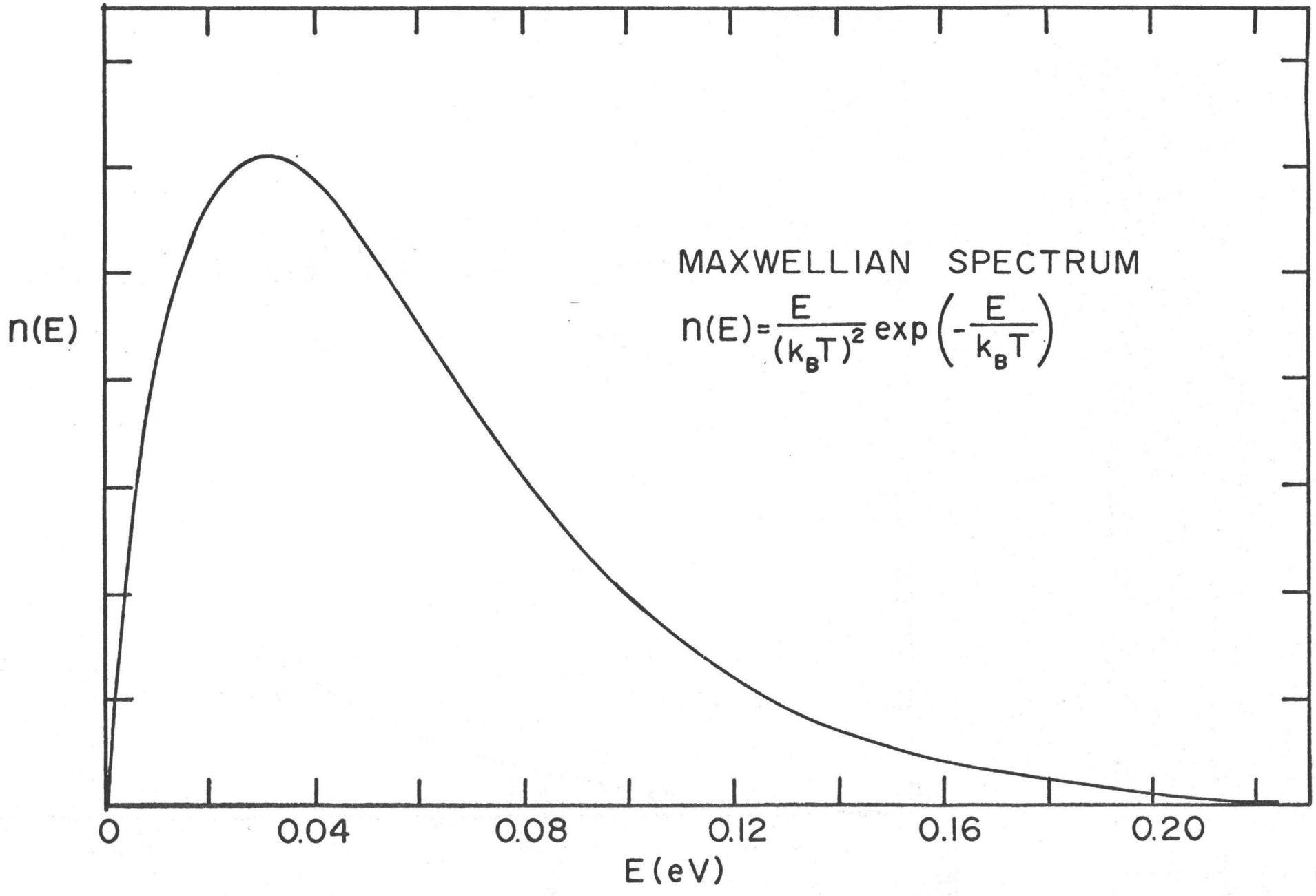

Fig. I-1 A typical Maxwellian spectrum from a nuclear reactor.

at present; the single crystal monochromator, used in conjunction with triple-axis spectrometers; and the neutron chopper monochromator, used in time of flight techniques. The latter type is basically a neutron velocity discriminator which allows only those neutrons with velocities within a specified range to pass through the monochromator. There are many interesting and ingenious variations of the basic chopper mechanism as outlined by Brugger (1965).

Of greater interest to the author is the single crystal monochromator. Such devices are, in general, far more economical in construction than the chopper and virtually free from any type of mechanical failure since the mechanism of energy selection is Bragg scattering.

Since efficiency is a critical factor in the selection of a crystal monochromator, one tries to choose a material with high coherent scattering cross-section and low absorption cross-section. Materials such as Be, Cu, Pb and pyrolitic graphite fall into this category.

In practice, it is desirable to have some knowledge of a calculated upper limit to the efficiency which one may then hope to approach in reality. It has been found by Brockhouse et. al. (1968), Dorner (1970), Dymond & Brockhouse (1970) and others, that efficiencies measured by experiments are consistantly lower than those predicted. It was the purpose of the experiments described in this thesis to gain some insight into this discrepancy and hence to lessen the gap between the upper limit and the efficiencies obtained by experiment.

CHAPTER II

THEORY

II-1. Simultaneous Reflections

As mentioned in the introduction, the mechanism for selecting a desired energy range from the total reactor spectrum is Bragg reflection and can be described by the familiar Bragg Law

$$n\lambda = 2d \sin\theta \qquad \text{II-1}$$

where n = the order of the reflection, λ = the wavelength associated with the scattered neutrons, d = the interplanar spacing, θ = the angle of incidence measured between the direction of the incident neutrons and the plane of reflection. For a particular crystal geometry, there may be more than one set of planes which satisfy the Bragg condition simultaneously. In terms of reciprocal space, the Bragg condition becomes

$$\underline{Q} = \underline{k}_o - \underline{k}' \qquad \text{II-2}$$

where $\underline{k}_o$ and $\underline{k}'$ are the incident and scattered wave vectors respectively, and $\underline{Q}$ is a reciprocal lattice vector. From Eq. II-2, it is clear that the Bragg condition is satisfied for all $\underline{k}'$ which terminate on any reciprocal lattice vector $\underline{Q}$, assuming a predetermined $\underline{k}_o$. This statement is interpreted geometrically for one simultaneous reflection, designated by $\underline{k}''$, in Fig. II-1 which represents scattering in an hypothetical reciprocal lattice. The Bragg condition is satisfied at all

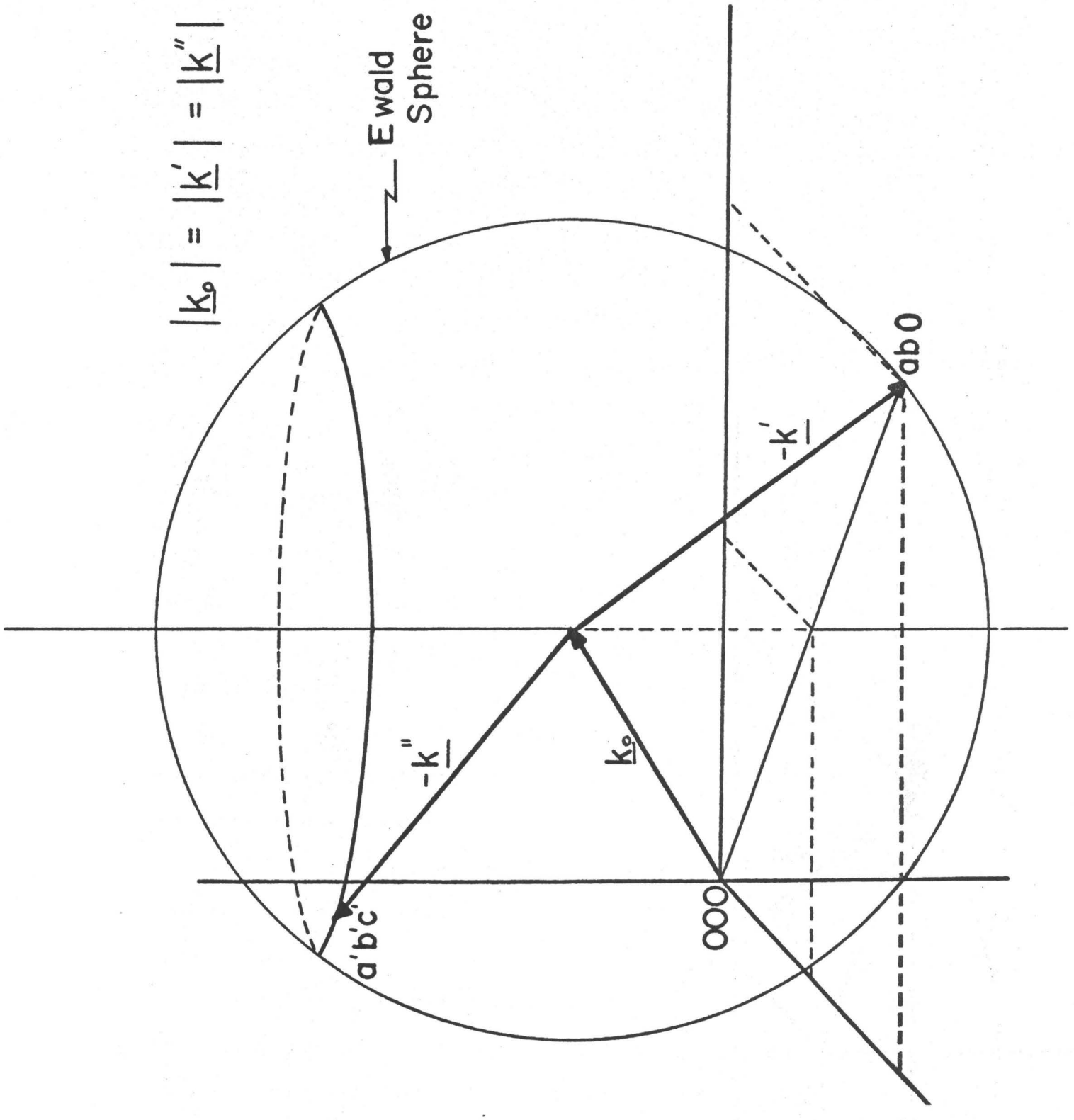

Fig. II-1 Scattering of neutrons in an hypothetical reciprocal lattice with one simultaneous reflection present.

reciprocal lattice points located on the surface of the sphere (Ewald sphere) swept out by $\underline{k}'$. In the example here, the desired and simultaneous reflections are designated (ab0) and (a'b'c') respectively. However, since each reciprocal lattice point may be considered as an equivalent origin, each scattered wavevector, $\underline{k}'$ and $\underline{k}''$, may be considered as the primary wavevector and hence may be scattered back into the original incident wavevector $\underline{k}_o$, and the complementary scattered wavevector $\underline{k}''$ or $\underline{k}'$. Thus, although neutrons, which are ordinarily available for reflection into the primary reflected beam, are in fact lost to the secondary reflected beam, there is a contribution returned to both the incident and primary reflected beams from the secondary reflected beam. Needless to say, the effects arising from more than one simultaneous reflection become very complicated and the calculation of the resultant loss of intensity by the primary reflected beam is very tedious.

Qualitatively, one expects the freqeuncy of occurrence of simultaneous reflections to be largest at low wavelengths, or large plane spacings, since in this limit, the radius of the Ewald sphere approaches its largest value and hence the number of reciprocal lattice points coincident with the sphere increases.

Simultaneous reflections have been investigated extensively for X-ray studies beginning with Renninger (1937). Although the fundamental principles governing simultaneous reflections are the same for X-rays as neutrons, their effect is much more noticeable in the case of neutrons since absorp-

tion is less significant than for X-rays and hence the neutrons can penetrate farther into the crystal, thus increasing the chance of being reflected by various families of lattice planes. Another important feature found in neutron studies is the "mosaic" width of the monochromators. This quantity is generally of the order of 30 to 40 minutes of arc which is far wider than most crystals studied by X-rays. This large width can cause overlapping in the wings of two different Bragg peaks which, for a perfect crystal, would not have occured and thus presented no problem.

The effects of simultaneous reflections occuring in neutron studies, have been investigated by several authors (Borgonovi and Caglioti, 1962; Willis, 1963; Moon and Shull, 1964). However, the general result seems to indicate that adequate calculations of the general situation are too difficult to carry out and hence one is restricted to making approximations which are not always applicable, or to selecting a crystal geometry such that the effects of simultaneous reflections are minimized.

II-2 Reflectivity of Neutrons off an Infinitesimal Perfect Single Crystal

Before studying the scattering of neutrons off a real crystal, it is informative and perhaps beneficial to first gain some insight into the fundamental processes involved in scattering. It can be readily shown that the ratio of the amplitude of a diffracted neutron beam to the amplitude of the incident beam for the (hkl) reflection from a unit cell

of a bravais crystal, is given by the structure factor, F, defined below

$$F^2 = \left|\sum_{b_j} b_j \exp(2\pi i \underline{Q}\cdot\underline{\rho}_j)\right|^2 e^{-2W} \qquad \text{II-3}$$

where b_j is the nuclear coherent scattering amplitude of the jth atom, $\underline{\rho}_j$ is its position vector in the unit cell, $\underline{Q}$ is the reciprocal lattice vector associated with the (hkl) reflection and W is the Debye Waller factor.

Using the structure factor F, one can follow the technique of James (1948, p.36) to calculate the amplitude of the reflected neutron beam at some point which is distant from the extended scattering surface under question. One finds that this quantity is given by

$$q = 2Nd^2F$$

where N is the reciprocal of the unit cell volume, d is the plane spacing, and F is the structure factor defined above.

The scattering of neutrons from a small, perfect crystal block is a coherent phenomenon since the intensity of such a reflection is determined by the addition of amplitudes of the neutron waves. The penetration of these waves into the crystal block is very limited due to the high attenuation of incident neutrons in the body of the crystal. As a result, the inner planes of the crystal contribute less to the reflected intensity than do the outer planes. Thus, when the crystal reaches a certain size, little or no gain in reflected intensity can be expected. This effect is known as primary extinction.

In the absence of primary extinction and absorption (ie.,

when considering a perfect crystal small enough such that it is essentially uniformly bathed in radiation) one can show, in the fashion of James, that the total reflected intensity per unit incident intensity per unit volume when the crystal is rotated through the Bragg position, is given by

$$Q = \frac{\lambda^3 N^2 F^2}{\sin 2\theta} \qquad \text{II-4}$$

where N is the reciprocal of the unit cell volume and F is the structure factor of the reflection defined above.

The no absorption approximation in such a small crystal block is quite adequate (Darwin, 1914) since the linear absorption coefficients for the copper crystals studied are of the order of 0.45 cm^{-1} and hence any reduction in intensity in a distance corresponding to the no primary extinction approximation ($\sim 10^{-4}$ cm.) is quite small.

In considering the case where the crystal thickness is large enough for primary extinction to occur, an approximate correction can be applied to the integrated intensity, Q, assuming the incident beam is reflected from the face of a large crystal slab (see Zachariasen, 1944 and DeMarco and Weiss, 1962). The corrected integrated intensity, Q', is given by Eq. II-5.

$$Q' = \frac{Q \tanh A}{A} \qquad \text{II-5}$$

where $A=\lambda N F t_o/\gamma_1$, t_o being the thickness of the crystal block, and γ_1 being the direction cosine of the angle between the incident beam and the surface of the crystal. The ratio Q'/Q, is defined as ε and the functional dependence of ε for copper is plotted against the crystal thickness, t_o, for (200) and (220)

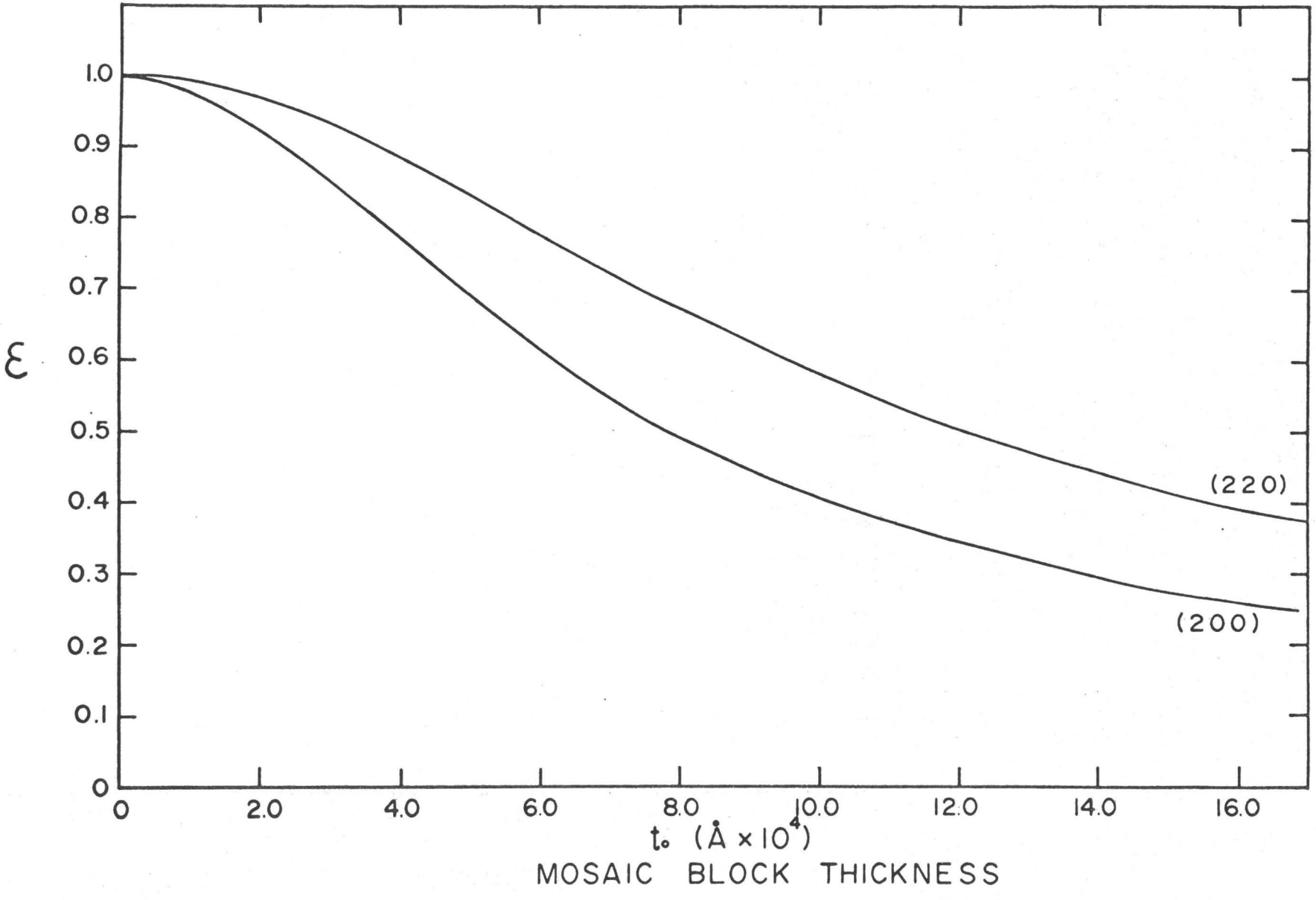

Fig. II-2 Primary extinction correction factor, ε, as a function of mosaic block thickness for the (200) and (220) reflections in copper.

reflections at room temperature in Fig. II-2. The figure shows the result that primary extinction is an increasing function of the plane index. Note also the rapid decrease in ε as the crystal thickness increases, ie., primary extinction increases.

II-3 Reflectivity of Neutrons off an 'Ideally Imperfect' Mosaic Crystal

Having briefly reviewed the reflecting properties of a small perfect crystal, one now constructs a model of a real crystal consisting of an assembly of these small crystal blocks, called mosaic blocks, randomly oriented about some preferred direction in the crystal. This highly idealized situation is believed to give an adequate macroscopic description of the effects caused by microscopic dislocations which occur throughout the crystal.

The model proposed by Bacon and Lowde (1948) for the calculation of reflected intensities of neutrons from mosaic crystals is essentially that of Zachariasen but modified from the X-ray to the neutron case. This model, hereafter called the B & L model, proposes a crystal with infinite lateral extent and finite thickness. The crystal itself is assumed to be mosaic with the constituant blocks so small that primary extinction is negligeable as well as absorption in the individual block, but there is an overall finite absorption when the total extent of the crystal is considered. Such an hypothetical crystal is termed 'ideally imperfect'.

The angular distribution of mosaic blocks is defined by the function $W(\Delta)$ such that one interprets $W(\Delta)d\Delta$ as the relative number of mosaic blocks, the normals to which lie between the angle Δ and $\Delta+d\Delta$, measured from the normal to the crystal surface. Δ is the angular distance from the Bragg position (ie., $\Delta=\theta-\theta_B$). Thus, as the neutron beam passes through the crystal, it will encounter mosaic blocks with the same orientation and hence the incident beam will be attenuated according to the density of mosaic blocks with identical orientation. This effect is called secondary extinction and is distinguishable from primary extinction by the fact that reflected contributions from different mosaic blocks add intensities (secondary extinction) while the contribution from individual mosaic blocks add amplitudes (primary extinction). For mathematical convenience, one assumes, after Zachariasen (1944), that the mosaic blocks can be manipulated into mosaic planes or layers, the reflecting power of which is $R = QW(\Delta)/\gamma_1$.

In considering the effect of an infinite crystal slab of thickness T on a pencil beam of neutrons, it is convenient to consider the power of the various neutron beams found at a depth t in the crystal. The set of differential equations below describes the processes in the crystal which attenuate the neutron beam. These equations are a more general version of the Bacon and Lowde (1948,1962) power equations which have been expanded by Moon and Shull (1964) to include the effects of simultaneous reflections.

$$\frac{dP_1(t)}{dt} = -\frac{P_1(t)}{\gamma_1}(\mu+R_{12}+\Sigma R_{1i}) + \frac{P_2(t)}{\gamma_2}R_{21} + \sum_i \frac{P_i(t)}{\gamma_i}R_{i1}$$

$$\frac{dP_2(t)}{dt} = C_1\frac{P_1(t)}{\gamma_1}R_{12} - C_1\frac{P_2(t)}{\gamma_2}(\mu+R_{21}+\Sigma_i R_{2i}) + C_1\sum_i \frac{P_i(t)}{\gamma_i}R_{i2}$$

$$\frac{dP_i(t)}{dt} = C_2\frac{P_1(t)}{\gamma_1}R_{1i} + C_2\frac{P_2(t)}{\gamma_2}R_{2i} - C_2\frac{P_i(t)}{\gamma_i}(\mu+R_{i1}+R_{i2}+\sum_{j\neq 1} R_{ij})$$

$$+ C_2\sum_{j\neq 1}\frac{P_j(t)}{\gamma_j}R_{ji} \qquad \text{II-6}$$

where C_1 and $C_2 = \mp$ for reflection and transmission geometry respectively (ie., Bragg and Laue scattering), $P_1(t)$ is the power of the incident neutron beam at a depth t in the crystal; $P_2(t)$ the power of the primary reflected beam; and $P_i(t)$, the power of the ith secondary reflected beam (ie., the i-2 simultaneous reflection); R_{ij}, the reflecting power of the reflection involving the incident and scatterd beams i and j respectively (see Fig. II-3); and μ is the linear absorption coefficient characteristic of the crystal. The boundary conditions imposed on this set of equations are as follows

$$P_1(0) = P_1(0)$$
$$P_i(0) = 0 \text{ transmission geometry}$$
$$P_i(T) = 0 \text{ reflection geometry} \qquad \text{II-7}$$

The exact solution to the above equations is very tedious for an arbitrary number of simultaneous reflections. Moon and Shull (1964) have made an approximate solution which is valid in the thin crystal limit (low absorption and low secondary extinction) but no attempt has been made to solve the power

equations in general terms. As pointed out by Moon and Shull, the usefulness of such a general solution is questionable when weighed against the labour involved. However, the exact solution of the power equations has been obtained in the presence of one simultaneous reflection. The solution thus obtained is frequently useful for two simultaneous reflections due to the high symmetry present out of the scattering plane in the reciprocal lattice. A more detailed description of this doubling of parasitic reflections is forthcoming in Chapter IV.

The solution in the absence of any simultaneous reflection is that obtained by Bacon and Lowde and given in Eq. II-8 below.

$$\frac{P_2(0)}{P_1(0)} = \frac{a}{(1+a) + \sqrt{1+2a}\,\coth[A\sqrt{1+2a}]} \quad \text{reflection}$$

$$\text{and} \qquad \frac{P_2(T)}{P_1(0)} = e^{-A(1+a)} \sinh(Aa)$$

$$= \frac{1}{2}\, e^{-\mu T/\cos\theta}\left(1-e^{-2\frac{Q\bar{W}(\Delta)T}{\cos\theta}}\right) \quad \text{transmission} \qquad \text{II-8}$$

where $a = \frac{Q\bar{W}(\Delta)}{\mu}$ and $A = \mu T/\sin\theta$. The solutions above were obtained under the assumption that $\gamma_1 = \gamma_2$, ie., the family of reflecting planes are parallel to the surface of the crystal slab. The general situation where the family of reflecting planes are at some oblique angle to the surface of the crystal is shown in Fig. II-3.

Because of the mosaic nature of the crystal, neutrons are reflected over an angular range, greater than the so called 'natural width' (Bacon and Lowde, 1948), when the crystal is rotated about an axis in the plane of reflection. The integrated

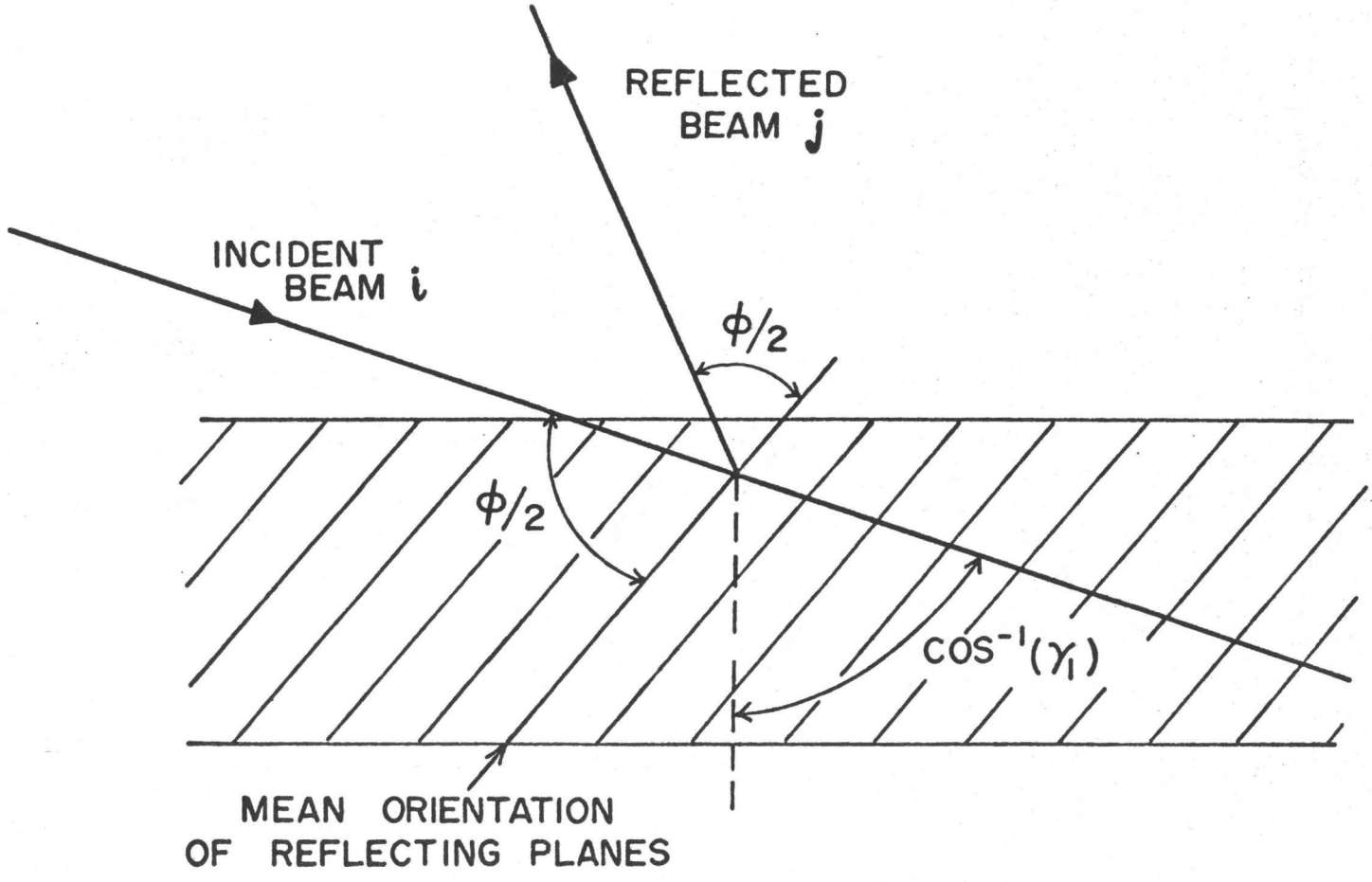

Fig. II-3 Geometry of Bragg reflection from an infinite crystal slab when the reflecting planes are at some oblique angle to the crystal surface.

reflectivity, R_θ, is then defined as the area under the resulting rocking curve per unit time, divided by the incident intensity per unit time. Thus,

$$R_\theta = \int_{-\infty}^{+\infty} \frac{P_2(0)}{P_1(0)}\, d\Delta \qquad \text{in reflection}$$

$$\text{and} \quad R_\theta = \int_{-\infty}^{\infty} \frac{P_2(T)}{P_1(0)}\, d\Delta \qquad \text{in transmission} \qquad \text{II-9}$$

II-4 Mosaic Block Distribution Functions

In the proposed model of a mosaic crystal, Bacon and Lowde, in the fashion of Zachariasen, assumed that the mosaic block distribution function was a Gaussian distribution characterized by a standard deviation η. Such a distribution was used since a knowledge of the form of the true distribution was not then, and is not now, available from experiment and thus, for lack of a better approximation, the Gaussian has remained.

In the thin crystal limit, it is expected from Eq. II-8 that the peak shapes obtained in a rocking curve would be proportional to $W(\Delta)$. Thus,

$$\frac{P_2}{P_1} \propto \frac{e^{-\Delta^2/2\eta^2}}{\eta}$$

and hence

$$\ln[\eta P_2/P_1] \approx -\frac{\Delta^2}{2\eta^2} + C \qquad \text{II-10}$$

Thus, if the mosaic distribution, and hence the peak shape, is Gaussian, the semi-log plot of Eq. II-10 should be linear.

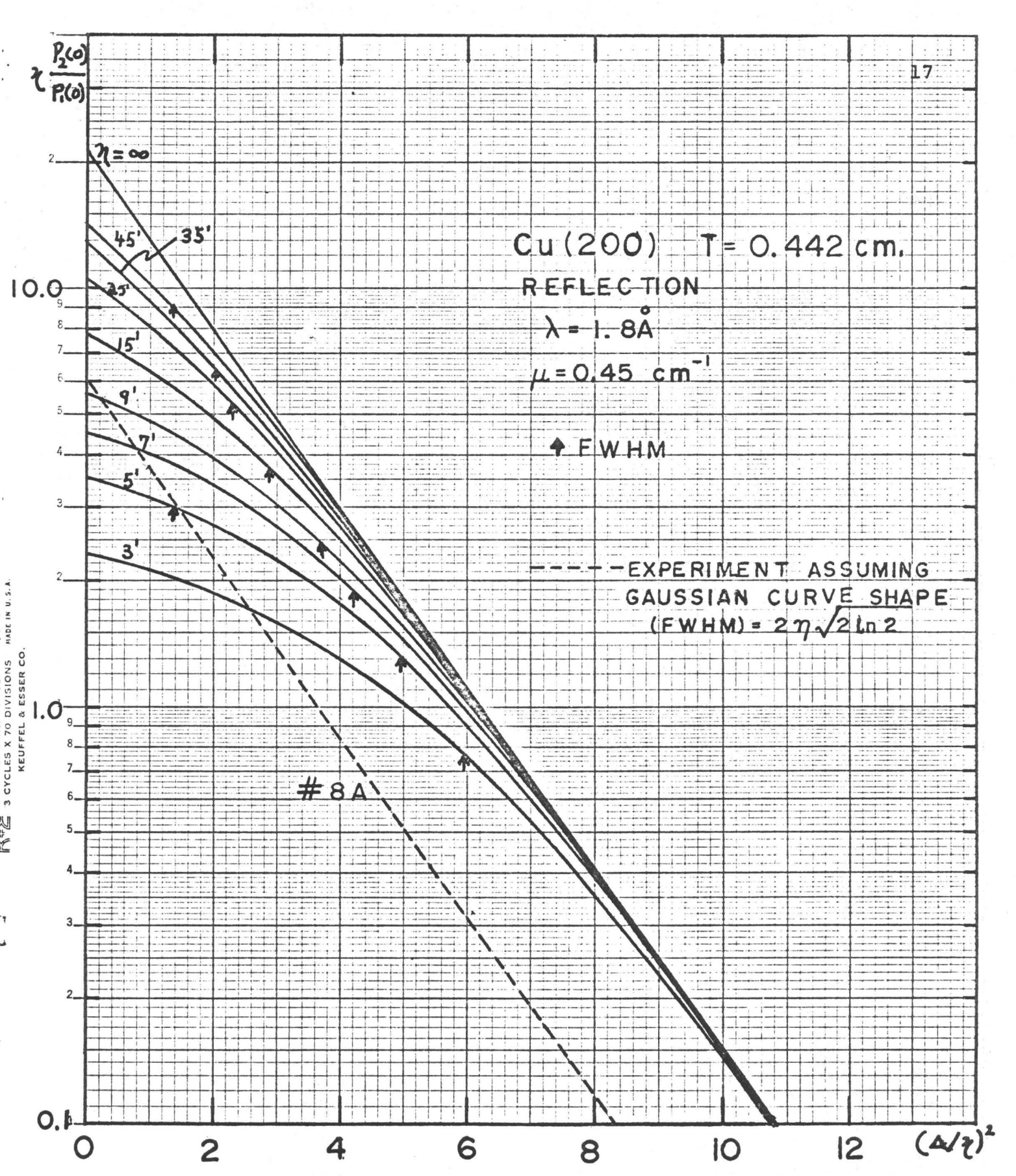

Fig. II-4 A plot showing how Bragg peaks approach a Gaussian shape as η increases.

However, as shown in Fig. II-4, the calculated curve shapes are not entirely Gaussian for thick crystals, the central portion deviating most strongly from this approximation. The points marked FWHM represent the positions of the FWHM on the abscissa to give an indication where peak shapes become Gaussian. This result as predicted by Bacon is due to extinction effects in the crystal, ie., the peaks are showing indications of saturation and thus flattening of the central portion occurs. However, the peak shapes that are actually observed in practice much more closely approximate a Gaussian shape (in reflection geometry) as indicated by the dotted line in Fig. II-4. As mentioned elsewhere (Dymond and Brockhouse, 1970) the ability to adequately match experimental and calculated curve shapes is important if one desires to make meaningful predictions of absolute integrated reflectivities which will establish realistic values of the achievable upper limit to R_θ.

The standard technique used to calculate the predicted integrated reflectivity is to adjust the mosaic distribution parameter, η, until one obtains agreement in one of the physical properties of the measured Bragg peak, usually FWHM. Such a technique is used since indirect measurements of η cannot be made with desired accuracy.

Table II-1 is a sample result obtained using the method described above for crystal #8A at a wavelength of 1.3 Å in reflection geometry. The parameters found in the third line of the table are, from left to right, the absorption coefficient

REFLECTIVITY (R) VS. MOSAIC SPREAD (ETA) FOR AN IDEALLY IMPERFECT ABSORBING CRYSTAL
COPPER (200) PLANE 0.442 CM THICK REFLECTION

ABMU = .80000 Q= .01348 D= 1.80740 WL= 1.30000 T= .44250 DW= .92000

S(J)	ROOTS(J)	R(J)	J	R(K)	K	ETA	FWHM
2.12143E+00	1.46	3.23	251	3.23	225	1.00	4.47012E+00
7.38454E+00	2.72	5.23	251	5.23	225	2.00	8.10022E+00
1.53942E+01	3.91	6.77	251	6.77	225	3.00	1.14303E+01
2.56759E+01	5.07	8.04	251	8.04	225	4.00	1.45204E+01
3.83818E+01	6.20	9.11	251	9.11	225	5.00	1.75505E+01
5.33450E+01	7.30	10.04	251	10.04	225	6.00	2.03405E+01
7.05121E+01	8.40	10.85	251	10.85	225	7.00	2.33106E+01
8.98444E+01	9.48	11.57	251	11.57	225	8.00	2.61607E+01
1.11313E+02	10.55	12.22	251	12.22	225	9.00	2.88908E+01
1.34895E+02	11.61	12.80	251	12.80	225	10.00	3.15008E+01
1.60573E+02	12.67	13.33	251	13.33	225	11.00	3.39909E+01
1.88333E+02	13.72	13.81	251	13.81	225	12.00	3.70810E+01
2.18104E+02	14.77	14.25	251	14.25	225	13.00	3.93911E+01
2.50057E+02	15.81	14.65	251	14.65	225	14.00	4.24211E+01
2.84004E+02	16.85	15.03	251	15.03	225	15.00	4.45512E+01
3.19998E+02	17.89	15.38	251	15.38	225	16.00	4.75213E+01
3.58035E+02	18.92	15.70	251	15.70	225	17.00	4.94713E+01
4.40210E+02	20.98	16.29	251	16.29	225	19.00	5.52915E+01
5.30518E+02	23.03	16.80	251	16.80	225	21.00	5.98516E+01
6.29918E+02	25.08	17.25	251	17.25	225	23.00	6.41717E+01
7.35400E+02	27.12	17.66	251	17.66	225	25.00	6.97519E+01
8.49950E+02	29.15	18.02	251	18.02	225	27.00	7.53320E+01
9.72559E+02	31.19	18.35	251	18.35	225	29.00	7.91721E+01
1.10322E+03	33.21	18.65	251	18.65	225	31.00	8.46323E+01
1.24192E+03	35.24	18.92	251	18.92	225	33.00	9.00924E+01
1.38865E+03	37.26	19.17	251	19.17	225	35.00	9.34525E+01
1.54342E+03	39.29	19.40	251	19.40	225	37.00	9.87927E+01
1.70622E+03	41.31	19.61	251	19.61	225	39.00	1.04133E+02
1.87704E+03	43.32	19.81	251	19.81	225	41.00	1.09473E+02
2.05589E+03	45.34	19.99	251	19.99	225	43.00	1.14813E+02
2.24275E+03	47.36	20.16	251	20.16	225	45.00	1.17453E+02
2.43764E+03	49.37	20.32	251	20.32	225	47.00	1.22673E+02
2.64054E+03	51.39	20.47	251	20.47	225	49.00	1.27893E+02

Table II-1

in cm^{-1}, the reflectivity Q in cm^{-1} as defined in Eq. II-4, the interplaner spacing in Å, the wavelength in Å, the crystal thickness in cm, and the exponential form of the Debye Waller factor e^{-2W}. Columns R(J) and R(K) are the calculated integrated reflectivities. The duplication is merely a check for convergance in the program. Columns J and K are indices used in the program and for present purposes should be ignored. Column ETA gives the value of mosaic spread parameter, η, in minutes of arc, used to calculate the integrated reflectivity which can be found to the left of column η. The FWHM of the calculated peak for the desired η is read, in minutes of arc, immediately to the right of column ETA. Columns S(J) and ROOTS(J) are the variance and standard deviation associated with the Bragg peak curve shape. These quantities are calculated from the second moment and the square root of the second moment respectively of the P_2/P_1 function defined in Eq. II-8.

Using the ROOTS(J) column, one can immediately determine how well the crystal under study, approaches the approximation leading to Equation II-10. In other words, if the quantity ROOTS(J) agrees with the quantity ETA, then the standard deviation of peak shape and the standard deviation of the mosaic distribution function are approximately the same and hence one has a good approximation for the thin crystal limit (or low secondary extinction). As expected, for large η(ETA), agreement between ROOTS(J) and ETA improves since one is approaching the low secondary extinction approximation described earlier in this chapter.

In an attempt to gain better agreement, a more suitable form for $W(\Delta)$ was sought. The Gaussian approximation implies that a single value of η must describe the interior state of the crystal. For an untreated crystal this approximation may be adequate but after the crystal is subjected to treatment as described in Chapter III, there is no reason to expect the effects of the deformations to be uniform. In other words, η may vary throughout the crystal.

Not wanting to stray too far from the Gaussian approximation, it was assumed that there exists a value of η, called η_o, which characterizes the crystal, but is only the most probable value of η in the crystal. In other words, η is distributed about η_o by some weight factor $g(\eta)$ which is assumed to be Gaussian and charactericed by the variance σ^2.

ie;
$$g(\eta) = e^{-(\eta-\eta_o)^2/2\sigma^2} \qquad \text{II-11}$$

By introducing this new distribution,we have introduced a new degree of freedom, σ. However, the justification of a particular choice of σ lies in the accuracy inherent in the model when one tries to predict results over a given wavelength range for a given σ.

Using the above weight factor, one finds that the probability that a given value of η, say η_i, occurs, is just

$$w_i = \frac{1}{\sqrt{2\pi}\eta_i} \; e^{-\frac{\Delta^2}{2\eta_i^2}} \; e^{-(\eta_i-\eta_o)^2/2\sigma^2}$$

Thus, the unnormalized distribution function of the mosaic blocks is just

$$W = \sum_i w_i$$

where the summation is over all possible values of η. If the spectrum of η is continuous, the distribution becomes

$$W(\Delta) = \int_0^\infty \frac{1}{\sqrt{2\pi}\eta} e^{-\Delta^2/2\eta^2} e^{-(\eta-\eta_o)^2/2\sigma^2} d\eta$$

which upon normalization, reduces to

$$W(\Delta) = \frac{\int_0^\infty \frac{1}{\eta} e^{-\Delta^2/2\eta^2} e^{-(\eta-\eta_o)^2/2\sigma^2} d\eta}{2.5066 \int_{-\eta_o}^{o} e^{-\xi^2/2\sigma^2} d\xi + 3.1415\sigma} \qquad \text{II-12}$$

(See appendix I)

Before proceeding further, one must note that the expression justdeveloped becomes physically unacceptable if the ratio σ/η_o gets too large. To more clearly understand the situation, refer to Fig. II-5 which shows the functional dependance of $g(\eta)$ for several values of σ and η_o. The model proposed implies a symmetric distribution about η_o as depicted in diagram (a). However, as η_o decreases, and/or σ increases one finds it necessary to truncate a significant portion of the distribution, as depicted in (b), in order to preserve the criterion that η be postive (the physical significance of a negative η escapes the author). It is a simple problem to show that the latter case can be avoided if one restricts oneself to the condition that $\sigma \leq 0.4\eta_o$. This restriction

ensures that truncation will not occur for more than 5% of the peak height crossing the $\eta=0$ boundary.

$$g(\eta) = \exp\left(-(\eta - \eta_o)^2/2\sigma^2\right)$$

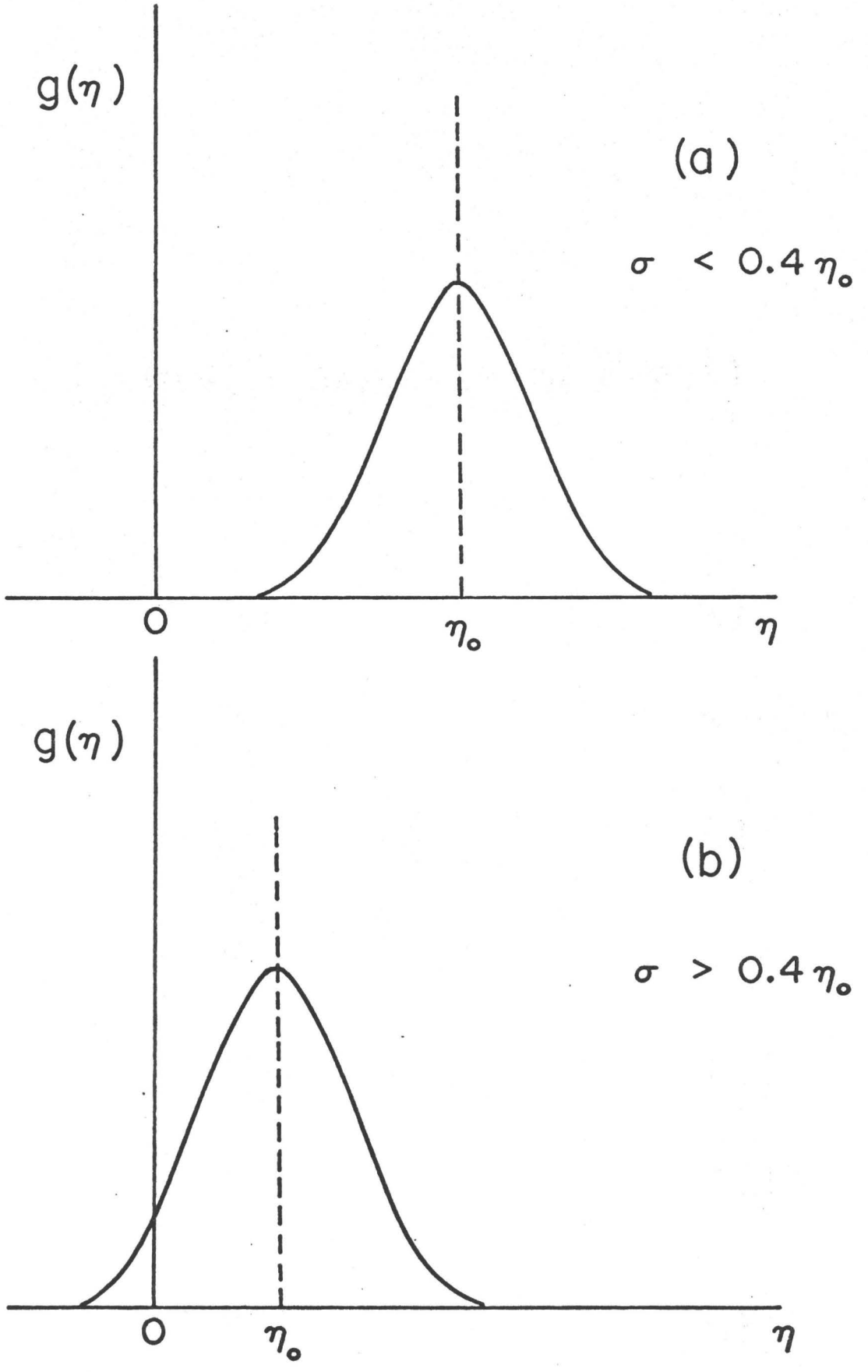

Fig. II-5 Non-Gaussian weight factor, $g(\eta)$, for the two cases $\sigma < 0.4\eta_o$ (a), and $\sigma > 0.4\eta_o$ (b).

CHAPTER III

EXPERIMENTAL AND APPARATUS

The experiments were carried out on the McMaster University triple-axis spectrometers at the McMaster reactor and the NRU reactor at Chalk River (Brockhouse et al, 1968). Fig. III-1 is a schematic diagram showing the geometrical configuration used in the experiments. The double monochromator shown in the figure is a property of the E-2 installation at Chalk River only, and not of the spectrometer used at McMaster. Although triple-axis spectrometers offer their main contribution in the field of inelastic neutron scattering, they lend themselves quite naturally to reflectivity studies, especially the Chalk River instrument since one has very rapid access to a continuum of neutron wavelengths because of the double monochromator system used. A Ge single crystal obtained from Alfa Crystals (Ventron) in Bradford, Pennsylvania, was situated as shown in the figure. The Ge crystal used was a circular disc approximately 6.4 cm in diameter and 0.037 cm thick with a (110) axis perpendicular to the face. The crystal slice was aligned with the (110) axis parallel to the face, up, such that a (311) and a (331) reflecting plane was readily accessible for the purpose described below. The function of this crystal was that of a secondary monochromator which would select from the incident beam, which was already a selected portion of the reactor spectrum, the desired

wavelength. Ge was selected for this purpose because of its lack of significant mosaic structure (<1" FWHM) such that the widths of any measured peaks were due only to the true widths of the sample and geometrical factors such as parallelism and collimation, and not to the width of the Ge monochromator. In order to minimize geometrical contributions to the measured widths, the plane of reflection in the Ge was chosen such that its plane spacing was as close as possible to the plane spacing of the sample copper crystal being studied. Thus, a Ge(311) reflection (d=1.706 Å) was used in conjunction with a Cu(200) reflection (d=1.807 Å) and a Ge(331) (d=1.298 Å) with a Cu(220) (d=1.278 Å). By using these planes, the condition of parallelism was satisfied, as shown in Appendix III, and the measured peak widths were due only to the true width of the sample and the collimation. All collimators used were Soller slits with an angular divergence of 0.0125 radians.

The beam from the Ge monochromator was then passed through an aperture 0.8 cm square into the analyzer housing of the spectrometer where the copper crystal to be studied was placed.

The sample crystals studied were slabs of approximate dimensions 15. 0 x 5.1 cm with thicknesses of 0.442 cm and 1.27 cm. They were grown by Research Crystals in Richmond, Virginia, in one of two orientations such that either a [200] or [220] major axis was perpendicular to the face of the crystal slab. Those crystals with a (220) face were aligned with a [220] axis up and those with a (200) face,

with a [200] axis up. The two sets of planes studied were those parallel and perpendicular to the face of the crystal. The former were studied in reflection geometry and the latter in transmission geometry, also known as Bragg and Laue geometry respectively. As received, the crystals had rocking curve widths of 6 to 10 minutes of arc (FWHM) and integrated reflectivities ranging from 1 to 3 minutes. The crystals were deformed in various ways, described in Table III-1, in a manner intended to improve their reflectivities without making their rocking curves too wide. Turberfield (1968) was able to increase the mosaic width, and hence the reflectivity, of his copper crystals by doping them with Be.

The Bragg peaks for each reflection were obtained by rocking the sample crystal against the stationary Ge monochromator while holding the detector in a stationary position. The angle designated θ is hereafter used to mean only the angle between the incident neutron beam and the desired plane of reflection (ie., either (200) or (220)).

The integrated reflectivity, defined as the area under the Bragg peak divided by the intensity per counting interval (N_o) of the beam incident on the specimen crystal, was measured as a function of wavelength for the crystals described in Table III-1 and the results compared with calculations based on the results of Chapter II. The absorption coefficient, μ, which is required to make the aforementioned calculations, was obtained by rocking the copper crystal through the Bragg peak with the He^3 detector in the "straight through" position

TABLE III-1

Description of treatment used to deform various copper crystals in order to improve their reflectivities

Crystal	Major Plane	Treatment		
		Type of Press	No. of Times	Stress(lbs/in^2)
* 8A	(200)	48" radius bend	6	500
		Straight press	1	2000
		36" radius bend	2	600
		36" radius bend	2	4000
		Straight press	1	10,000
		-Crystal was sliced down the centre on a band saw to make 2 thinner crystal slabs.		
		-Various other treatments which proved ineffective were tried (eg. temperature shock treatment).		
* 9	(200)	Straight press	1	5000
15	(220)	Untreated		
16	(220)	36" radius bend	2	3000
		Straight press	1	4000

* As treated by E. D. Hallman (Brockhouse et al, 1968)

After each bending, the crystal was subjected to a straight press at the same stress as was used for the bending

and hence μ was calculated, assuming that the attenuation of neutrons through the crystal obeys an exponential decay law (ie., $N=N_o e^{-\mu x}$).

Informative discussions concerning various techniques for measuring reflectivities as well as precautions and approximations which are useful in many circumstances have been discussed by many authors (Bacon,1955; Burbank, 1964; Caglioti, 1964; Egelstaff, 1965; Arndt & Willis, 1966; Popovici et al., 1969).

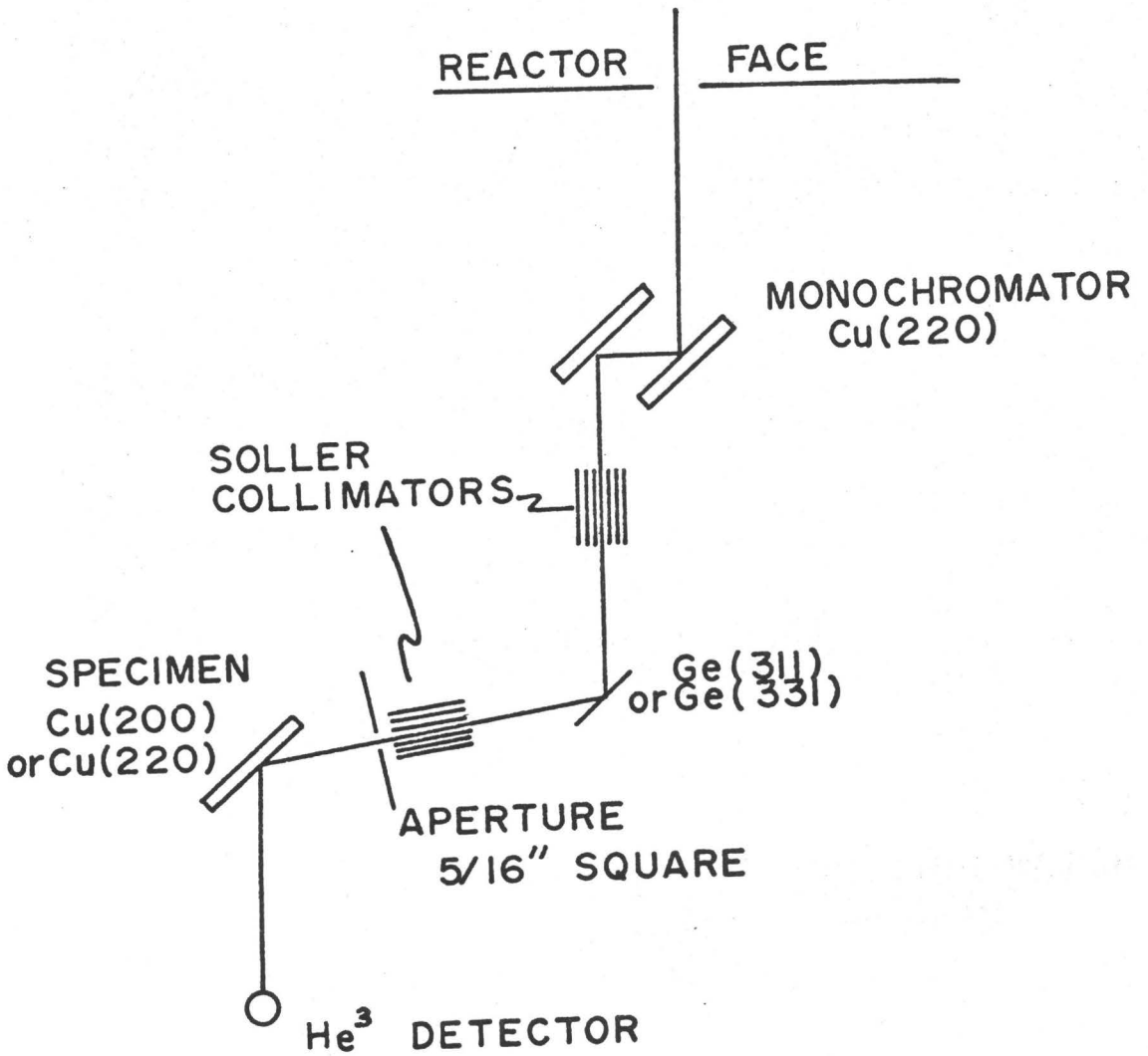

Fig. III-1 Schematic diagram of apparatus used in the experiments.

CHAPTER IV

RESULTS AND DISCUSSION

The integrated reflectivity of each crystal, defined in the previous chapter, was measured in transmission as well as reflection geometry for each wavelength studied, the results of which are plotted in Figures IV-1 to IV-10. Before discussing these curves in detail, it is informative to briefly discuss the effects of the various processes described in Chapter II, on the integrated and peak reflectivities. The solid and dashed lines of the above mentioned figures represent theoretical curves for the approximations tending towards;

(1) no secondary extinction or simultaneous reflections ($\eta = 49'$).

(2) no absorption or simultaneous reflections ($\mu = 10^{-4}$ cm^{-1}, $\eta = 8'$ or $4.7'$).

(3) no simultaneous reflections ($\mu = 0.45$ cm^{-1}, $\eta = 8'$ or $4.7'$).

(4) no simultaneous reflections and the Debye Waller factor unity ($2W = 0$).

It becomes clear from Fig. IV-1, that the greatest reduction in calculated intensity arises from absorption at low wavelengths (< 0.7 Å) and from secondary extinction at longer wavelengths. For copper, the Debye Waller factor contribution appears to be the least significant for the lower order (200) reflection but more important for the higher

order (220) reflection, as expected.

The results verify experimentally that R_θ, peak height, and the FWHM associated with the Bragg peaks, all increase in value with increasing wavelength, at least over the wavelength range studied. Also, the peak reflectivities, and to a lesser extent the integrated reflectivities, were higher for crystal #9 than for #8A in the reflection geometry and vice versa in the transmission geometry. This result arises directly from the fact that crystal #9 is more than twice as thick as #8A and hence, in reflection geometry, a larger volume of crystal can be irradiated for #9 but in transmission, the neutron path length is much longer and hence absorption plays a larger role in reducing the reflected intensity from the thicker crystal.

In transmission geometry, saturation of the peak height to a specified value is quite apparent. The particular value involved for a given crystal thickness is determined entirely by the degree of absorption. For example, in the absence of any absorption, the peak height saturates to 0.5 for any crystal thickness. However, when absorption is included, one expects the peak height to approach some value determined by μ and T and then decrease with increasing wavelength. Figures IV-4 and IV-8 clearly show that the B & L model does predict the above phenomonon, however, it has not been conclusively observed in experiment since the main effect occurs for wavelengths greater than about 1.8 Å and not enough experimental data has been obtained for this region.

The solid irregular line labelled "paraffin moderator experiment" in Fig. IV-1 shows the integrated reflectivity obtained from the sensitivity function by A. P. Roy (1970). In this experiment (Brockhouse, 1958), monochromatic neutrons were thermalized in a paraffin block placed on the specimen table. The analyser Bragg angle was then varied and the number of counts per unit time was recorded as a function of this angle. The integrated reflectivity was then extracted assuming a Maxwellian distribution for the neutrons scattered from the block, with appropriate corrections for second order effects. The results thusly obtained were then normalized. The agreement between this method and the method described throughout this thesis is quite good and serves to substantiate the validity of the method used.

The open triangles and squares represent calculated reflectivities obtained from the B & L model using measured values of μ. The appropriate η's were obtained by matching experimental and calculated FWHM. Introduction of the effective absorption coefficient has greatly improved agreement with experiment over the ordinary B & L model. However, it is quite clearly shown that matching FWHM yields calculated values of R_θ and peak height which are too high. But, if instead, R_θ is matched at one particular wavelength, then η is determined and can be accurately used to calculate R_θ over the rest of the wavelength spectrum (see Fig. IV-5, $\eta = 6'$). The latter procedure, although adequate for predicting R_θ, is in fact very poor in predicting the curve shape since the FWHM's no longer

match, and the peak height is greater than for the calculation with η = 8' (see Fig. IV-6). This result appears to be quite general for all crystals studied and will be treated in detail later in the text.

The results shown in Fig. IV-9 and IV-10 are of special interest. Here, one is able to directly observe the effects of mechanical treatment of a crystal as outlined in Chapter III. The closed circles represent experimentally determined reflectivities of crystal #15 in reflection. This crystal may be taken as quite representative of crystal #16 before treatment since it has been found that all untreated crystals studied had approximately the same properties. A comparison of Fig. IV-9 and IV-10 indicate that upon treatment, the gain in peak height is substantially lower than the gain in R_θ, indicating a marked increase in mosaic spread (from about 6' to 18' FWHM).

In transmission geometry, one finds an indication in Fig. IV-10 that the peak reflectivity of crystal #16 does decrease in value with increasing wavelength beyond the point of maximum peak height.

Another interesting feature of Fig. IV-9 is the general relationship between the values of R_θ obtained in reflection and those obtained in transmission. It appears that for a crystal thickness of 1.27 cm, R_θ in transmission is, generally speaking, only about 50% of the value in reflection. Since it is generally very useful to be able to use either geometry, one must choose a monochromator of optimum thickness such

that the reflectivities obtained in either geometry are brought to a maximum. Such a situation arises with the McMaster spectrometer at McMaster. Here, the monochromator used is similar to crystal #16 and is aligned such that for a given scattering angle, two wavelengths can be obtained, one by scattering from the (220) plane in reflection and the other from the (200) plane in transmission.

The monochromator used in the system at present is 1.27 cm thick. It is believed that a more efficient system could be employed by using a crystal with a thickness of about 0.6 cm. By analogy with the results obtained for crystals #8A and #9, one would not expect a substantial loss in intensity in the reflection geometry by using a thinner crystal but one would definitely expect an increase in reflectivity in transmission geometry. For example, in considering the (200) plane in reflection from crystal #9, T = 1.27 cm, it has been found that for λ = 2.0 Å, 98% of the incident neutrons were removed from the incident beam at peak intensity whereas only 86% were removed when crystal #8A was used. However, because of internal attenuating processes in the crystal (ie., absorption, multiple scattering, etc.), only about 55% of the incident neutrons were recovered from each crystal. Thus, for λ = 2.0 Å there is no substantial difference in the efficiencies of the crystals. However, at the other end of the wavelength spectrum ($\lambda \sim$1.0 Å), the efficiencies have dropped to 23% and 32% for the thin and thick crystals respectively. Although the

difference involved at this low wavelength is rather large, one would expect somewhat better correlation by using a crystal with thickness of about 0.6 cm. In transmission, one finds that approximately 38% (peak height) of the incident neutrons are recovered after reflection at λ = 1.8 Å from crystal #8A, but only about 28% are recovered from #9 whereas the efficiencies at λ = 1.0 Å are approximately the same at about 20%. Using the B & L model, one can perform calculations which indicate the similar sort of change in efficiencies with a crystal having a [220] major axis. Thus, one would expect the optimum crystal thickness to be between 0.442 and 1.27 cm, perhaps about 0.6 cm. In choosing the appropriate thickness, one should bear in mind that the thicker the crystal used, the higher the background encountered.

Another interesting feature is found in Fig. IV-9 and IV-10. In transmission geometry, excellent agreement is obtained between experiment and the B & L model for both peak and integrated reflectivities whereas in reflection geometry, agreement occurs only with R_θ and not with peak height. For those cases where agreement is good; in terms of R_θ, peak height, and FWHM, it should be noted that peak shapes are quite different, the calculated shapes more closely approximating rectangles while the measured shapes resemble triangles.

It was found that measured absorption coefficients varied considerably with wavelength for some crystal geometries and less so for others. However, at the higher wavelength

end of the spectrum ($\lambda \sim 2$ Å), the measured values of μ were approximately the same for all geometries studied, ie., $\mu \sim 0.45$ cm^{-1}. The R_θ vs λ curves all show the presence of dips corresponding to wavelengths where the measured values of μ do not vary smoothly with wavelength but vary quite erratically. This wavelength variation is attributed to the presence of simultaneous reflections, the effects of which can substantially lower neutron diffraction intensities. Reductions in intensity arising from simultaneous reflections of as much as 15% have been encountered (Caglioti, 1964). The presence of such simultaneous reflections is readily detectable by observing the transmission of neutrons through the sample crystal as it is rocked through the Bragg position. At this point, it is necessary to explain an upcoming inconsistency in the text. Calculations dealing with the reciprocal lattices of crystals with a [200] major axis were carried out as though the major axis was a [020] axis and hence the following discussion assumes that the planes parallel to the surface of the crystal are (020) planes. Of course the physics remains unchanged and it is hoped that no confusion will arise as a result of this change in notation.

Fig. IV-11 depicts the transmission curve and the Bragg peak obtained using crystal #8A in reflection for $\lambda = 1.3$ Å. As shown in the figure, three distinct, overlapping dips were found in the transmission curve in the angular range about the centre position of the Bragg peak. The centre dip in the transmission curve, occuring at $\theta = 21.2^\circ$ is caused

by the depletion of neutrons from the incident beam as a result of the desired (020) reflection. The dip on the low angle side of the (020) reflection arises from two (131) reflections and the dip on the high angle side from two (111) reflections (Dymond and Brockhouse, 1970). Similar peaks were obtained for crystal #9 but with significant changes in transmission intensity because of its greater thickness. That these tertiary reflections are those identified above becomes clear when one observes the processes occuring in the reciprocal lattice while rocking through the Bragg peak. Fig. IV-12 (a) is a view of the (001) plane in the reciprocal lattice of copper. The solid arrows labelled $\underline{k}_i$ and $\underline{k}_f$ are the incident and scattered wave vectors involved in the (020) reflection. The broken arrows labelled $\underline{k}_i'$ and $\underline{k}_f'$ are the incident wave vector and the component in the (001) plane of the scattered wave vector to the (131) and (13$\bar{1}$) reciprocal lattice points. At the particular wavelength in question, $\lambda = 1.3$ Å, the incident wave vectors $\underline{k}_i$ and $\underline{k}_i'$ are less than one degree apart (measured in the (001) plane) such that both reflections occur in the Bragg scan, the occurance of the (131) and (13$\bar{1}$) reflections being expected at $\theta = 20.2^\circ$. Fig. IV-12 (b) represents the (001) plane in three dimensions. The purpose of this three dimensional figure is to point out the pairing of simultaneous reflections arising from the symmetry which exists to either side of the (001) plane. Thus, any simultaneous reflections out of the plane occur in pairs, an effect which reduces the

intensity of the (020) reflection even further.

The effects of simultaneous reflections are not localized with respect to wavelength. In fact, in the example quoted above, the (131) and (111) simultaneous reflections affect the (020) reflection over the wavelength range from about 1.3 Å to 1.4 Å. The most noticeable decrease in intensity is expected for λ = 1.34 Å since this is the wavelength at which the (020),(131),(13$\bar{1}$),(111), and (11$\bar{1}$)reflections overlap completely. At higher wavelengths, the (111) peaks shift to lower values of θ while the (131) planes shift to higher values. Table IV-1 lists the significant simultaneous reflections encountered for λ = 1.0 Å to 2.0 Å for all crystal geometries studied. The table shows the presence of two very important simultaneous reflections, a (200) and a (020), for crystals with a (220) major axis in the reflection geometry. These reflections are important since their presence is felt over the entire wavelength region studied. They are not peripheral reflections, that is, the centre portion of each peak is coincident with the central portion of the desired (220) peak rather than with some portion of its wings. Thus, one would expect the reflected intensity of the (220) face to be substantially reduced by the other two reflections. This effect is of immediate importance since the E-2 installation at Chalk River employs a system of two parallel (220) copper crystals. As mentioned by Hallman (1969), the effect of these reflections can be reduced by tilting the monochromators

TABLE IV-1

Bragg reflections present for various crystal geometries studied in the wavelength range from 1.0 to 2.0 Å

1.0	1.1	1.2	1.3	1.4	1.5	1.6	1.7	1.8	1.9	2.0	
$(3\bar{1}\bar{3})$ $(3\bar{1}3)$ (020) $(4\bar{2}\bar{2})$ $(4\bar{2}2)$ $(33\bar{3})$ (333) $(44\bar{2})$ (442)	(240) $(0\bar{2}0)$ $(2\bar{2}0)$	$(31\bar{3})$ (313) (020)	$(13\bar{1})$ (131) (020) $(1\bar{1}\bar{1})$ $(1\bar{1}1)$	$(1\bar{1}\bar{1})$ $(1\bar{1}1)$ (020) $(13\bar{1})$ (131)	$(33\bar{1})$ (331) (020) $(3\bar{1}\bar{1})$ $(3\bar{1}1)$	(020) $(20\bar{2})$ (202) $(22\bar{2})$ (222) (400)	(020)	[001] UP (020)	(020)	$(31\bar{1})$ (311) (020)	(020) REFLECTION & TRANSMISSION
(002)	$(\bar{1}31)$ $(3\bar{1}1)$ (002)	(002) (040) (042) $(22\bar{2})$ (224) (400) (402) (440) (442)	(002)	(002) (240) (420)	(002)	(002)	(002)	[110] UP (113) (002) $(11\bar{1})$	(002)	(002)	(002) TRANS-MISSION
(331) (020) (200) (220)	$(\bar{2}02)$ $(\bar{2}04)$ $(\bar{2}\bar{2}2)$ $(\bar{2}\bar{2}4)$ $(0\bar{2}2)$ $(0\bar{2}4)$ (020) (042) $(2\bar{2}2)$ $(2\bar{2}4)$ (200) (220) (242) (402) (422)	(020) (200) (220)	(020) (200) (220)	(020) (200) (220)	(020) (200) (220)	(020) (200) (220)	(131) (311) (020) (200) (220)	[110] UP $(\bar{1}11)$ $(1\bar{1}1)$ (131) (020) (311) (200) (220)	(020) (200) (220)	(020) (200) (220)	(220) REFLECTION

WAVELENGTH (Å)

out of the (110) plane. This tilting procedure has been shown by O'Connor and Sosnowski, (1961) and Blinowski and Sosnowski, (1961), to be effective in eliminating, or at least reducing, the effects of many simultaneous reflections.

Crystal #16 represented a problem in trying to evaluate an appropriate absorption coefficient. The transmission curves obtained in reflection geometry were not solely due to the desired (220) reflection as mentioned above, but rather to the combination of a (220), (200), and (020) reflection. Fig. IV-13 shows such a transmission curve for λ = 1.6 Å. Clearly, one can only estimate the position which would give the number of neutrons passing through the crystal in the absence of the (220) reflection since one is visually unable to separate the effects of the three reflections present. This problem did not occur for crystals #8A and #9 since at the wavelengths studied, one could adequately separate the effects of simultaneous reflections from the desired reflection and an appropriate value of μ could be obtained (see Fig. IV-11). It should be mentioned, just as a point of consistency, that although the values of μ used for crystal #16 in reflection were all greater than 0.45 cm^{-1}, it was found that the base lines of the transmission curves do, themselves, occur for μ's of about 0.45 cm^{-1} in the central and higher wavelength regions.

In passing, it should be pointed out that the reflections listed in Table IV-1 affect the intensities of the desired

reflections in vastly varying degrees. Some reflections are strongest in the wings of the desired reflection while some are strongest in the central portion of the peak itself.

Once the simultaneous reflections had been identified, the power equations (Eq. II-6) were solved in the presence of one simultaneous reflection where possible. Restricting oneself to only one simultaneous reflection is not as restrictive a procedure as it may seem since it has been found that for a given specimen orientation, the reflected intensity of neutrons is generally affected by no more than one type of non peripheral simultaneous reflection. Thus, using the example of Fig. IV-11, one can solve the power equations for the two separate types of simultaneous reflections; ie., the (111) and the (131), and combine the results to obtain the curves of Fig. IV-14 (a) since the (111) and (131) reflections have no appreciable overlap. Also, the fact that there are two (131) and (111) reflections presents no great obstacle in the one simultaneous reflection approximation. The pairing of simultaneous reflections can be accounted for by replacing the reflection coefficients, R_{13} and R_{23}, by $2R_{13}$ and $2R_{23}$ respectively, except in the third equation which remains unchanged (see Appendix II).

Fig. IV-14 draws a comparison between experimental curve shapes and those obtained by the solution of Eq. II-6 for crystal #8A (λ = 1.3 Å), as previously mentioned, and crystal #16 (λ = 1.6 Å). The most noticeable features of

both figures (a) and (b) is the lack of agreement between experimental and calculated relative intensities. The transmission curves predict a much larger attenuation of the incident neutron beam by Bragg reflection than appears in the actual experiments. Even when one neglects the effect of pairing simultaneous reflections, the predicted intensities are much greater than those obtained by experiment. The difference encountered is much greater for #8A than for #16. This does not necessarily mean that crystal #16 is closer to being "ideally imperfect" than #8A but rather that #16, due to its greater thickness, is closer to saturation in the peak than is #8A. It is interesting to note that the calculated effects of the (111) reflections appear to have no effect on the (020) reflection, and that the (131) reflections have only slightly more. Obviously, the effect would increase if the wings of the calculated curve shapes were broader. On the other hand, the effects of the (200) and (020) reflections on the (220) reflection, shown in (b), are much greater. Several interesting features can be found in the second figure. Firstly, it appears that although only a small change occurs in the transmission curve when one goes from the non-pairing to the pairing of simultaneous reflections, there is a much more substantial change in the peak intensity of the Bragg peak ($\sim$35% increase). Secondly, the calculated transmission curve for crystal #16 has a much different line shape than that found in experiment, the experimental line shape being sharply peaked at the centre

with extremely broad wings. This shape was typical of those found at all wavelengths for the particular (220) reflection studied. It is believed that the unusual peak shape encountered is due to a slight misorientation out of the reflecting plane. Although the crystal was aligned as well as possible, a slight shift out of the (001) plane would cause the (020) and (200) reflections to shift in opposite directions on the $\theta-\theta_B$ axis. A third feature made evident in (b) is the change of Bragg peak shape as the effects of the simultaneous reflections are introduced. The effect of introducing the non-paired simultaneous reflection approximation is to increase the FWHM from 17' to 22' and by introducing the paired simultaneous reflections, the FWHM is further increased to 29'.

One fortunate feature inherent in the Bragg peaks and transmission curves when measured in the transmission geometry is that one can obtain a good measure of reflecting efficiency on a relative scale. Such a measure of the efficiency of crystal #16 is obtained from Fig. IV-15. These figures are presented to show the similarity between the transmission curve and the Bragg peak in the transmission geometry. In this geometry, one finds that the effects of absorption can be accounted for by a multiplicative factor antecedent to the Bragg intensity (see Eq. II-8). Thus, one may plot the transmission and Bragg curves on a scale reduced by the quantity $\exp(-\mu T/\cos\theta)/2$ as the figures show and if no scattered neutrons are lost en route to the detector, then the two curves should

be mirror images of each other, ie., the number of neutrons scattered equals the number of neutrons detected. Dorner (1970) was first to use this type of plot. The results obtained here indicate that the peak intensities encountered saturate to their maximum value over a large portion of the wavelength spectrum studied. The mirror-like symmetry between the curves is very important in terms of experimental technique since the existence of this symmetry ensures that one is detecting all the scattered neutrons. In this type of experiment, good geometry is essential since the loss of a portion of the scattered beam can affect the experimentally determined absolute reflectivity.

To present, the calculated reflectivities have been obtained assuming that the mosaic blocks were distributed according to a Gaussian distribution about some average direction in the crystal. Using this approximation, one finds, in theory, that the predicted curve shapes of the Bragg peaks tend to flatten across the top since the crystal ideally is reflecting, in total, all the neutrons which are available for reflection after all internal attenuating processes have acted. As one would expect, the flattened peaks become most evident for the thicker crystals and/or at longer wavelengths since these are the conditions for which secondary extinction prevails. In the experiments carried out to date, no curves with such shapes have been observed. Fig. IV-16 shows a typical experimental Bragg peak compared with the calculated curve shapes for various values of mosaic distribution parameter, η, using

the proposed Bacon and Lowde model.

In the reflection geometry, the experimental peak values are consistantly lower than those predicted from theory for all values of η which might be conceivably characteristic of the crystal. However, in the transmission case, the calculated and measured peak values agree well as both approach the saturation point for the wavelengths depicted. The absorption coefficient was not measured in the transmission geometry for crystals #8A and #9. Instead, the values of μ obtained in the reflection geometry were used, under the assumption that both crystal were aligned such that two mutually perpendicular (200) planes were themselves perpendicular to the direction of the incident beam of neutrons. This restriction was ensured for crystal #8A but not for crystal #9 since the latter crystal is the analyser crystal most frequently used in the McMaster University spectrometer at Chalk River and it was decided not to realign the crystal so that only the reflection plane was well aligned with the transmission plane being approximately 3 degrees from the normal. As a result, the effective absorption coefficient is lower in the transmission geometry since the removal of symmetry in the crystal decreases the effect of simultaneous reflections. Thus, the measured peak height often exceeds the calculated peak height in transmission geometry for crystal #9 but not for crystal #8A.

Another general property of the measured Bragg peaks is the tendency for the slope of the wings of the experimental peaks to be less than those obtained from calculation. It has

been found that such observations are consistent for all experimental peaks measured.

Thus, the B & L model fails to adequately predict curve shapes which resemble those curves obtained by experiment. As a result of this discrepency, the B & L model was altered in an attempt to decrease the slope of the wings and at the same time decrease the peak height. The former change was realized but the opposite effect to that desired resulted in the latter alteration. The results were obtained by using the mosaic block distribution function developed in Chapter II. Fig. IV-17 is a display of calculated Bragg peaks obtained using the non-Gaussian distribution of mosaic blocks for neutrons with λ = 1.8 Å. In comparison with Fig. IV-16, it becomes clear that the non-Gaussian approach alters the B & L model in the correct manner, ie., sharpening the peaks and broadening the wings. In reflection however, the peak heights are greater in the non-Gaussian case than the B & L case. As a result, one must resort to scaling procedures on the calculated curve shapes to provide an adequate match between predicted and measured curves. It has been found that the calculated curves in the transmission geometry can be made to coincide quite adequately with experiment without having to resort to scaling procedures as shown in Fig. IV-17. The discrepancy between the transmission and reflection case is believed to be associated in some way with the interpretation of μ, the effective absorption coefficient, and with the degree of sat-

uration of the Bragg peak. Two methods have been successfully used to scale the curves in reflection; one method is the direct multiplicative scaling of the intensities, and the other method is the scaling of Q in an attempt to introduce primary extinction. The former method is considered first.

The closed circles of Fig. IV-18 are the calculated points using the appropriate scale factor for the reflection geometry and a scale factor of 1 for the transmission geometry. The curves represent calculated and experimental Bragg peaks at a sequence of wavelengths in both reflection and transmission geometry. The solid lines represent the experimental curve shapes. The calculated points are presented as points rather than dotted lines as is done with the upcoming figures IV-19 and IV-20, merely to emphasize the agreement between theory and experiment. In this figure, several interesting features concerning the wavelength variation of Bragg peak shapes become evident. It is noticed that in reflection geometry, the curve shapes of crystal #8A are accurately predicted using $\eta = 9'$ and $\sigma = 3'$ for λ greater than about 1.4 Å, but for wavelengths less than this, agreement in curve shape begins to suffer. Also, the curve shapes obtained from experiments at these lower wavelengths exhibit a different overall profile, the peaks being somewhat flatter and the wings less steep than the wings at higher wavelengths. However, upon examining the peak shapes for the transmission case, it is found that agreement is best at low wavelengths (1.0 to 1.5 Å) and agreement lessens for

wavelengths longer than this. Thus, the tendency away from agreement is opposite in the two cases of reflection and transmission. The scaling factor used, in reflection, appears to increase in value for increasing wavelength, the greatest change occurring for small λ where peak shapes are the poorest match. Scaling Bragg peaks in this fashion yields very good agreement between calculations and experiment and may be useful in practical terms when certain properties of a crystal are desired. However, from a physical point of view, this method is rather unsatisfactory since no physical basis is used which justifies direct scaling procedures.

The second type of scaling procedure does have a physical basis. Generally speaking, one neglects the effects of primary extinction by assuming that the mosaic block sizes are small enough to exclude the effect. Larson and Corey (1969) have found in their experiments, which were designed to study the effects of extinction upon annealing a cold worked copper crystal, that primary extinction was indeed negligeable for their crystals. Unfortunately, the concept of a mosaic block is highly idealized and hence, it is very difficult to obtain a meaningful value for the block size. Gay et al. (1953) and Brogren (1969) were able to get approximate block sizes ($\lesssim 10^{-4}$ cm) by relating dislocation density to the number of mosaic blocks per unit volume. In the forthcoming discussion, it was necessary to introduce mosaic blocks whose sizes were about six times greater than those obtained by the above authors.

Fig. IV-19 depicts the fit obtained using $\eta=9'$ and $\sigma=3'$ for crystal #9. The dotted lines represent the calculated curve shapes and the solid lines, the experimental peaks. The appropriate value of ε is indicated at each wavelength and for a particular value of λ, the same ε was used in both reflection and transmission geometries. The results of scaling Q by this procedure are similar in every respect to those obtained by direct scaling including the tendency away from agreement for low λ in reflection and large λ in transmission. As mentioned earlier, the lack of agreement between calculated and measured peak heights in the transmission case is the result of using inappropriate values of μ obtained in the reflection geometry. One possible explanation for the cause of the discrepencies described above is related to a possible variation of the degree of deformation throughout the crystal since the volume of the crystal observed in the experiment is wavelength dependent (see Fig. IV-22). In other words, for an incident neutron beam of given diameter the volume of crystal irradiated decreases with increasing wavelength in the transmission geometry. Thus if the crystal is not uniformly distorted throughout its volume, one would expect variation of η and/or σ with wavelength, the net effect being the change of curve shape in the manner described above. Preliminary experiments seem to substantiate such a variation, however, the observed change is rather small. Whether or not the observed variation is enough to affect the desired result is yet to be determined in the light of future experiments. Dorner (1970) was able to adequately

describe a similar variation of the degree of deformation in large single crystals by describing the crystal with a set of three layers, each with a different mosaic width. Although his treatment was used to study the effects of the surfaces of an unetched crystal, it should be feasible to expand his method to describe variations of mosaic spread deep within the crystal.

As was done with crystal #8A, a direct scaling fit was also applied for crystal #9. The results are not included here since the results obtained differ only marginally from the fit obtained by scaling Q. Fig. IV-20 is the same sort of plot as IV-19, for crystal #16. The results encountered for this crystal differ from those of the previously mentioned crystals in that excellent agreement between calculations and experiments occurs for the whole wavelength region in reflection geometry, and poor agreement occurs in transmission geometry. It was found that the best fit was obtained using $\eta=6'$ and $\sigma=2'$. Once, again, the value of ε used at a given wavelength was the same for reflection as for transmission.

In comparison with crystal #9, the scaled value of Q required to attain agreement in reflection for #16 was less. This result is not unexpected since if primary extinction is indeed involved, then the higher order (220) reflection should be less affected than the (200) reflection as shown in Fig. II-2. But it was just mentioned that the ε used in reflection was also used in transmission. Since the (220) and (200) reflections are affected by primary extinction to a different extent (Fig. II-2), then using one ε for reflection and transmission is not justified. Using Fig. II-2, an appropriate ε was

established for the (200) reflection in transmission geometry, knowing the ε required for the (220) in reflection.

Using the ε obtained in this fashion, new peak shapes were calculated in transmission but it was found that these peak shapes were very insensitive to a variation in ε because of the high degree of saturation. The curve shapes obtained using the new ε are represented by the dotted lines at λ=1.0, 1.5, and 2.0 Å. Thus, the effect of introducing a more realistic value of ε for the (200) reflection in transmission geometry is quite small and does not appreciably alter the curve shapes obtained using the ε established from the curves in reflection geometry.

Fig. IV-21 is a plot of the wavelength dependence of ε for crystal #9 and #16. For #9, ε varies approximately linearly with λ as shown by the dark squares and extrapolation to λ=0Å yields $\varepsilon \gtrsim 1.0$. On the other hand, the wavelength dependence of ε for crystal #16 although varying approximately linearly up to about 1.6 Å shows a definite departure from a linear dependence at higher wavelengths. One can only speculate whether extrapolation to 0Å will yield an $\varepsilon \simeq 1.0$ or not but it does appear quite probable. It was mentioned earlier that there was difficulty in accurately determining μ in reflection geometry for crystal #16. If the values of μ chosen were not truly representative of the absorption present, then the resultant value of ε would also be non representative of the true situation.

This fact must be kept in mind when trying to interpret just how ε depends on λ. In order to clearly understand this last statement, we recall that in the B & L model, the quantity Q' always appears with μ and $W(\Delta)$ in the following way $\underset{\mu}{Q}'W(\Delta) = \varepsilon\underset{\mu}{Q}W(\Delta)$. Thus by using an inappropriate μ, one is able to obtain the same curve shape by adjusting ε, as one would obtain if the correct ε and μ had been used in the first place. Such would not be the case if it were not for the fact that the Bragg peak shape is relatively insensitive to a variation of μ in the quantity $\mu T/\sin\theta$.

For example, the open triangles of Fig. IV-21 were determined under the assumption that no simultaneous reflections were acting such that μ was determined by interpolating the base line of the transmission curve smoothly over the dip corresponding to the (220) reflection. As a result, μ was found to have a representative value of about 0.45 cm^{-1}. Using these newly determined values of μ, the calculated curve shapes were matched to the experimental shapes by adjusting ε to the values shown in the Figure. The curve shapes using the two different sets of ε and μ were identical except for very minor details arising from the slow response of the quantity $\mu T/\sin\theta$. The most interesting feature of the newly determined ε values is the fact that they take on an approximately linear dependence with λ which is almost coincident with the line produced by crystal #9.

If primary extinction is indeed occuring in the individual mosaic blocks and if the values of μ shown in Fig. IV-19 and 20 are truly representative, then since crystals #9 and #16 underwent similar mechanical treatment, one would expect the size of the mosaic blocks to be approximately the same for both crystals. In conjunction with Fig. II-2, one finds that predicted block sizes do agree quite well. For example, consider λ=1.5 Å. For the (220) reflection of crystal #16, $\varepsilon \sim .74$. This value corresponds to a mosaic block size of about 6.7×10^4 Å. Similarly for the (200) reflection of crystal #9, ε=.55 which corresponds to a block size of about 7.0×10^4 Å. According to the model proposed in Chapter II, the fact that ε is wavelength dependant implies that primary extinction is also wavelength dependant contrary to predictions by Zachariasen (1948). The physical significance of wavelength dependent primary extinction is not readily comprehensible since such a dependence implies that the size of the constituent mosaic blocks is a function of the neutron wavelength used to study them.

There are several possible explanations for a wavelength dependant ε. Firstly, it is possible that the model used to account for primary extinction is too highly idealized to adequately represent the true situation. In other words, the approximation of mosaic planes does not describe, in a realistic way, the dislocations whose boundaries form what are interpreted as mosaic blocks.

Secondly, the wavelength dependence of ε may be

related to the choice of η and σ for a given wavelength. Recalling that there is evidence that the deformation of treated crystals might vary appreciably through the volume of the crystal, then a variation of η and σ would imply a variation in ϵ since the curve shapes would be changed. Such a change in η and σ was tried in order to match the low wavelength Bragg peak shapes but in doing so, it was found that the ϵ required to fit the new peaks varied only slightly from the original value. Perhaps, a mosaic block distribution function which is dependent on position in the crystal might affect the desired change in ϵ, however, it is believed that the former explanation (ie., the inadequacy of the model) is the more probable of the two.

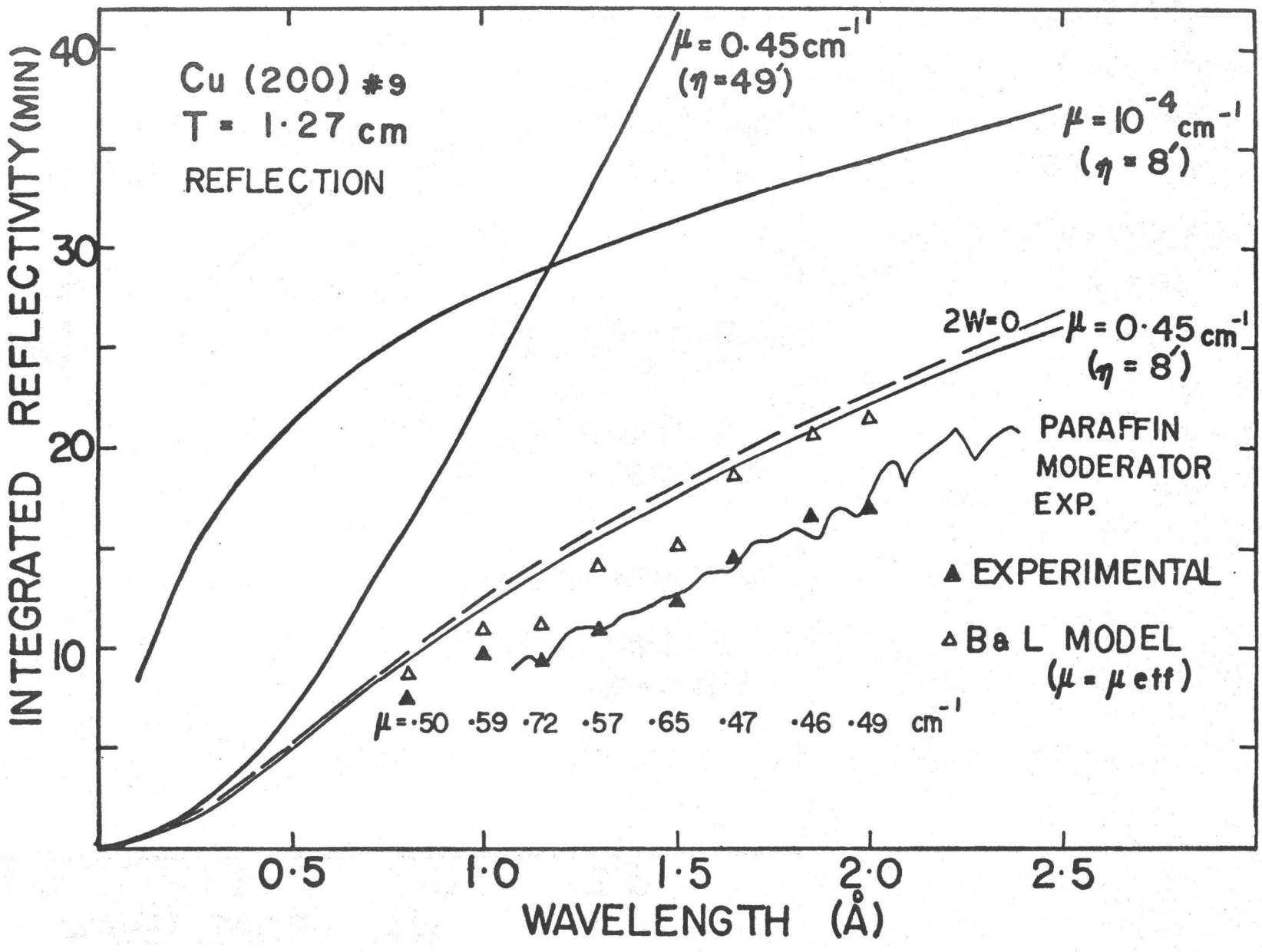
Cu (200) #9
T = 1·27 cm
REFLECTION
μ = 0·45 cm⁻¹
(η = 49′)
μ = 10⁻⁴ cm⁻¹
(η = 8′)
2W=0
μ = 0·45 cm⁻¹
(η = 8′)
PARAFFIN
MODERATOR
EXP.
▲ EXPERIMENTAL
△ Ba L MODEL
(μ = μ eff)
μ = ·50 ·59 ·72 ·57 ·65 ·47 ·46 ·49 cm⁻¹
INTEGRATED REFLECTIVITY (MIN)
40
30
20
10
0·5
1·0
1·5
2·0
2·5
WAVELENGTH (Å)

Fig. IV-1

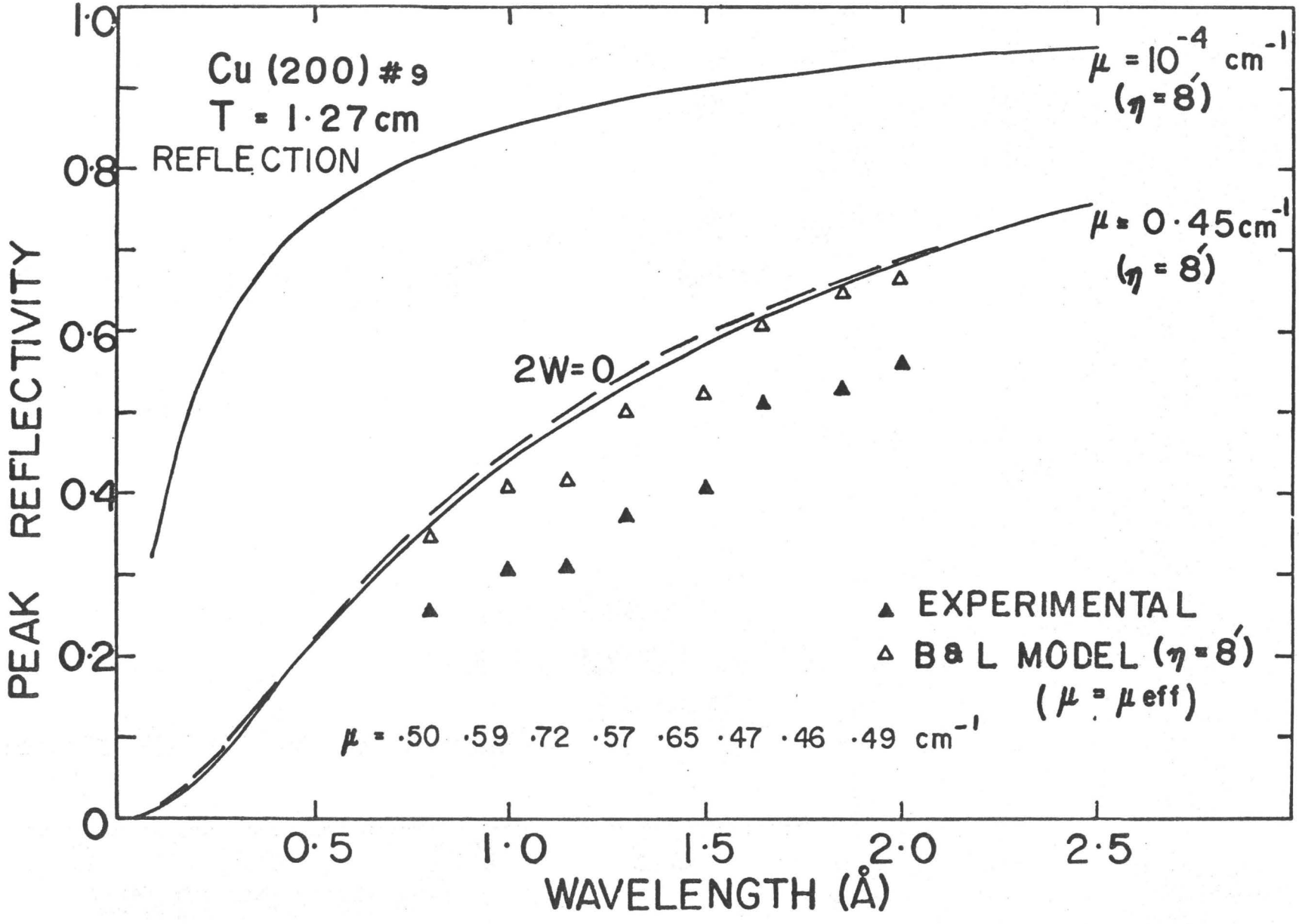
Cu (200) #9
T = 1·27cm
REFLECTION
μ = 10^-4 cm^-1
(η = 8′)
μ = 0·45cm^-1
(η = 8′)
2W=0
▲ EXPERIMENTAL
△ B & L MODEL (η = 8′)
(μ = μeff)
μ = ·50 ·59 ·72 ·57 ·65 ·47 ·46 ·49 cm^-1
PEAK REFLECTIVITY
WAVELENGTH (Å)
0
0·2
0·4
0·6
0·8
1·0
0·5
1·0
1·5
2·0
2·5

Fig. IV-2

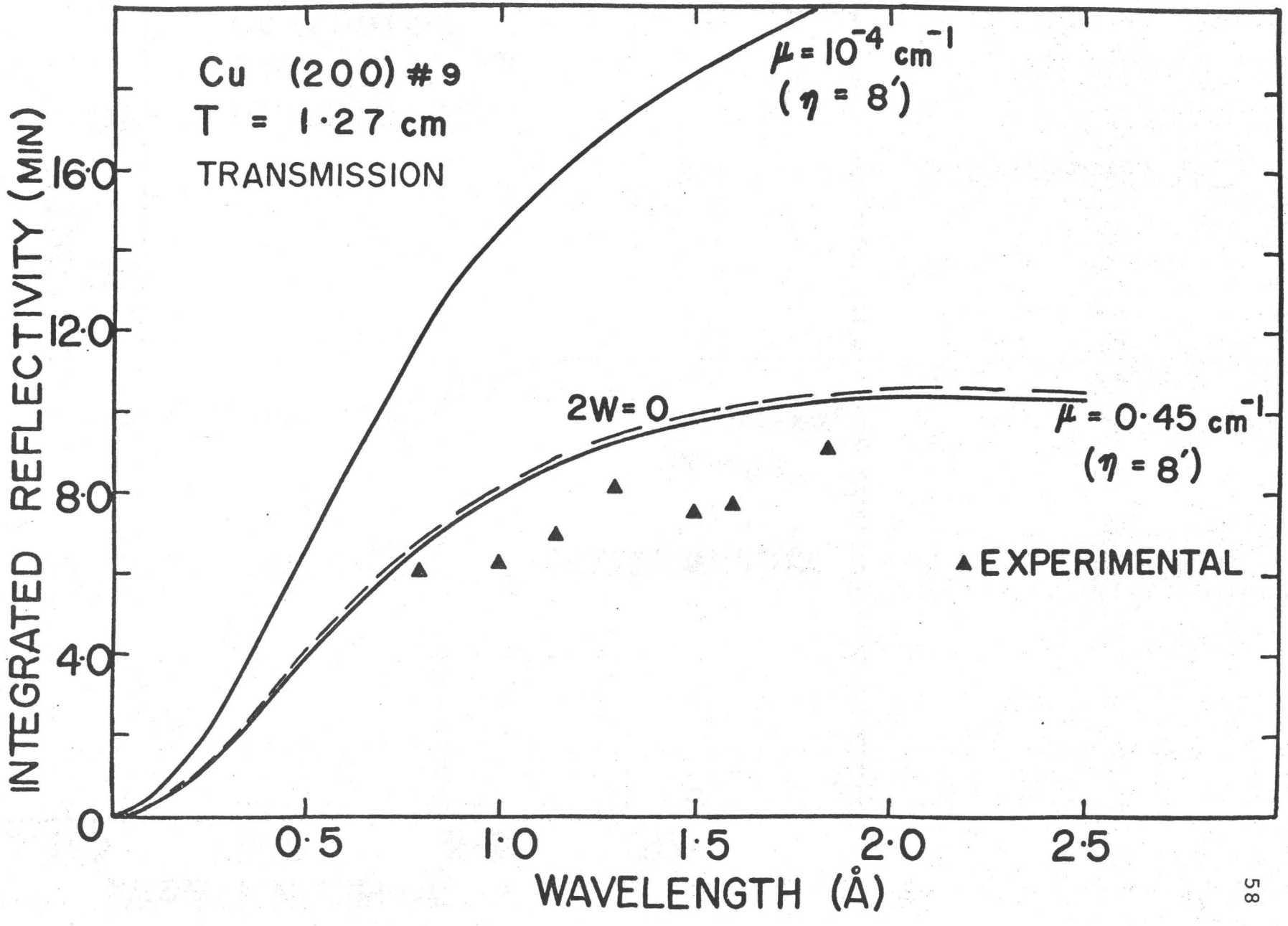
Cu (200) #9
T = 1·27 cm
TRANSMISSION
μ = 10⁻⁴ cm⁻¹
(η = 8′)
2W = 0
μ = 0·45 cm⁻¹
(η = 8′)
▲EXPERIMENTAL
INTEGRATED REFLECTIVITY (MIN)
0
4·0
8·0
12·0
16·0
0·5
1·0
1·5
2·0
2·5
WAVELENGTH (Å)

Fig. IV-3

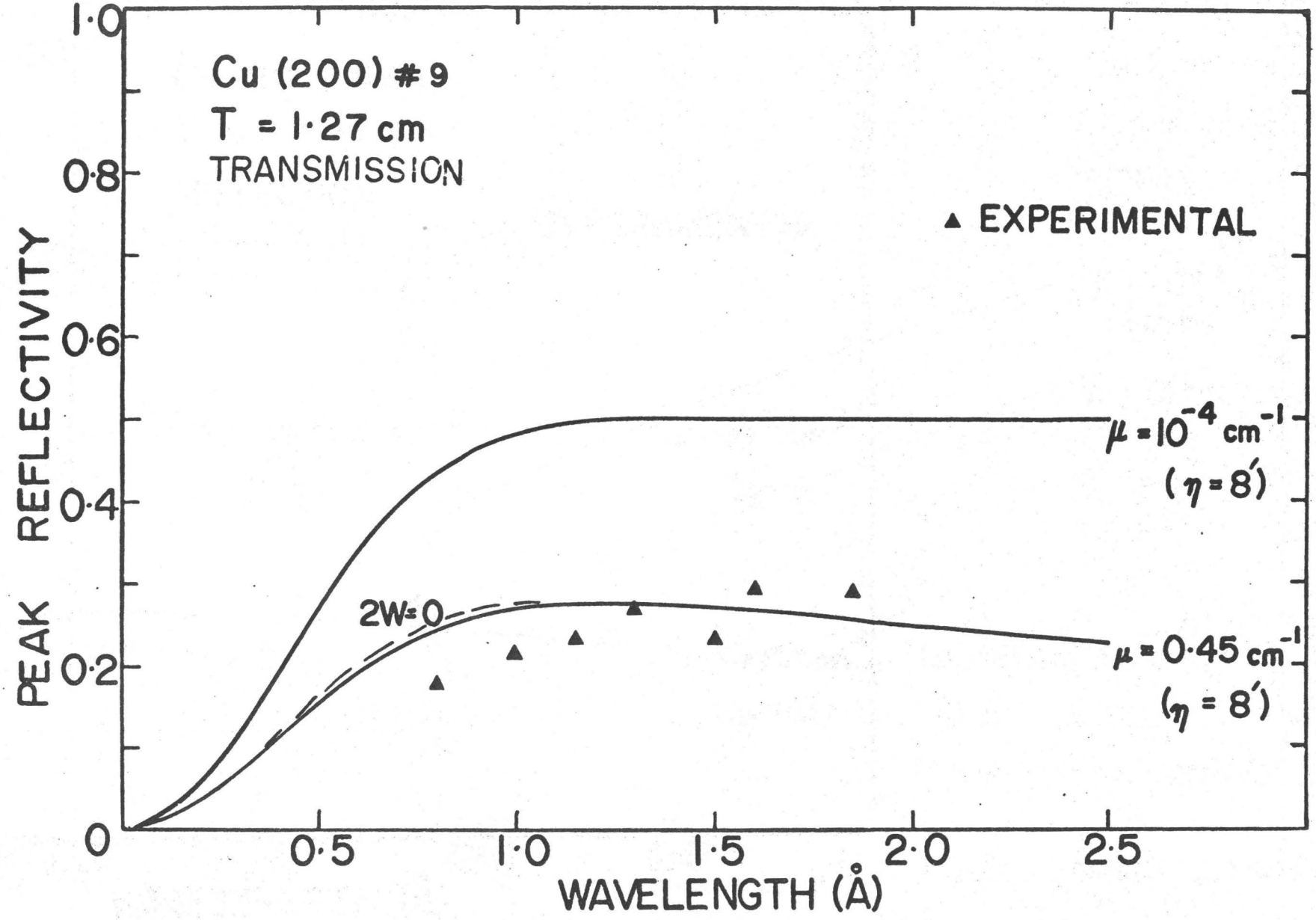
Cu (200) # 9
T = 1·27 cm
TRANSMISSION
▲ EXPERIMENTAL
PEAK REFLECTIVITY
WAVELENGTH (Å)
1·0
0·8
0·6
0·4
0·2
0
0·5
1·0
1·5
2·0
2·5
2W=0
μ = 10⁻⁴ cm⁻¹
(η = 8′)
μ = 0·45 cm⁻¹
(η = 8′)

Fig. IV-4

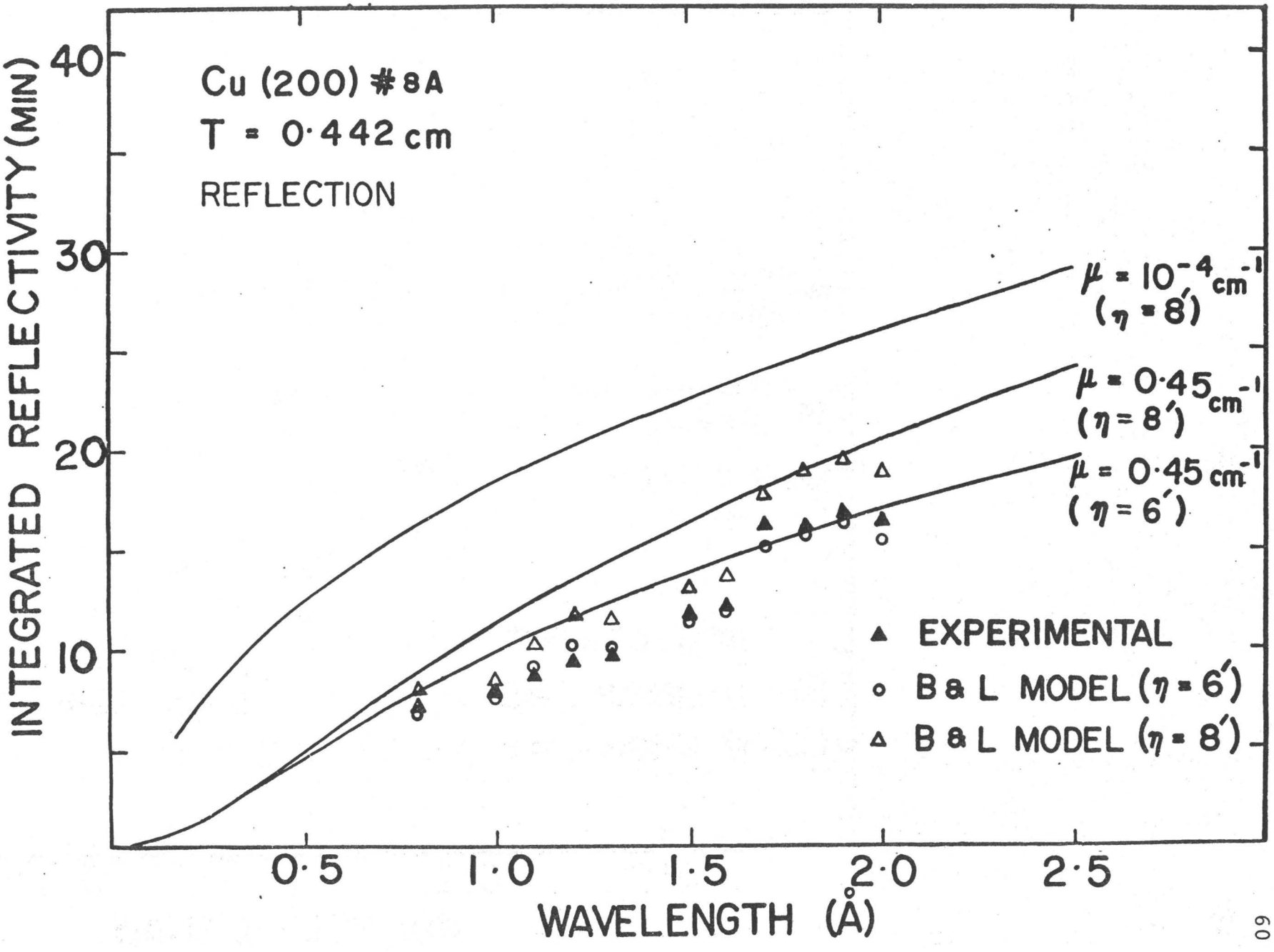
Cu (200) #8A
T = 0·442 cm
REFLECTION
INTEGRATED REFLECTIVITY (MIN)
40
30
20
10
0·5
1·0
1·5
2·0
2·5
WAVELENGTH (Å)
μ = 10⁻⁴ cm⁻¹ (η = 8′)
μ = 0·45 cm⁻¹ (η = 8′)
μ = 0·45 cm⁻¹ (η = 6′)
EXPERIMENTAL
B & L MODEL (η = 6′)
B & L MODEL (η = 8′)

Fig. IV-5

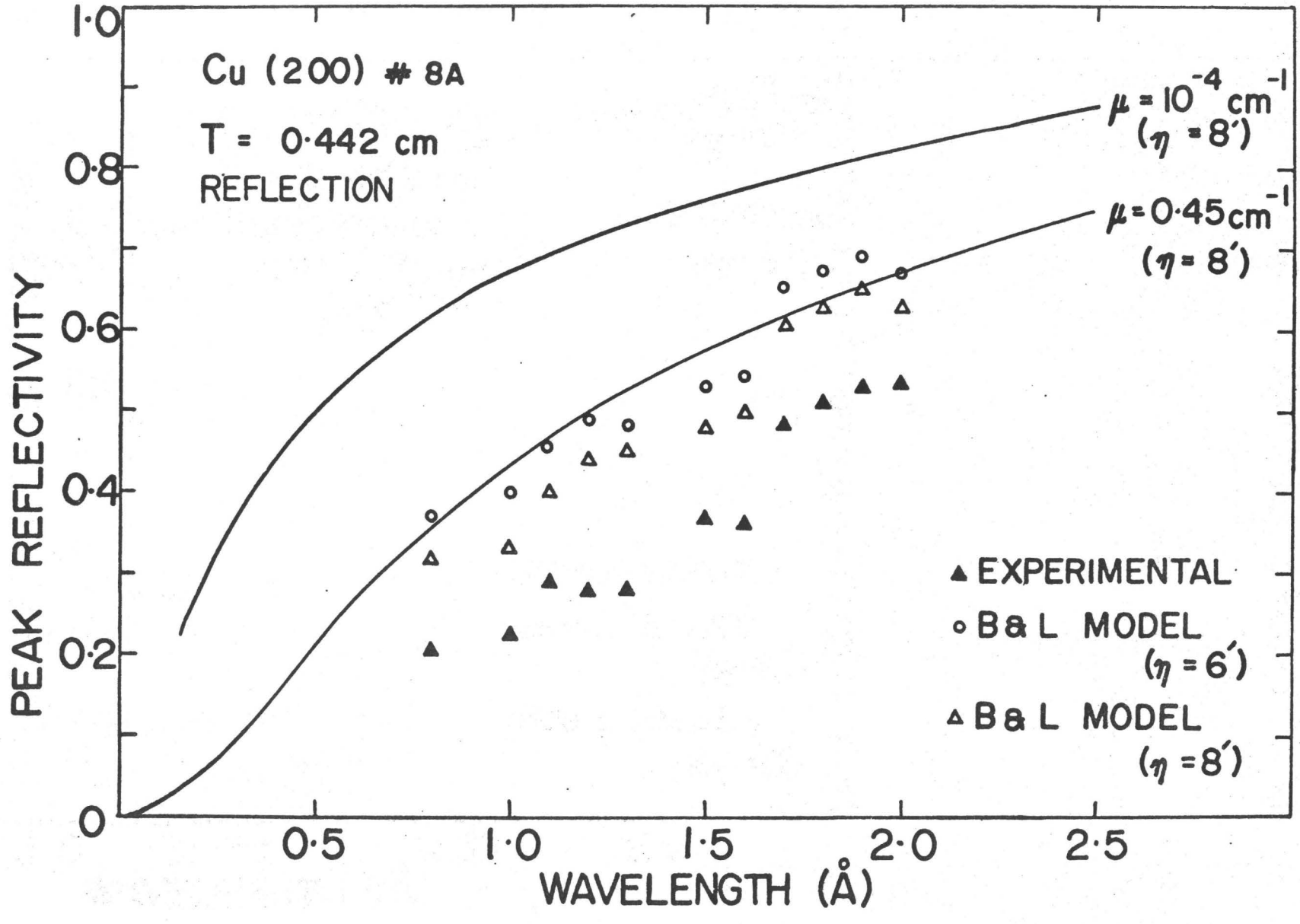
Cu (200) # 8A
T = 0·442 cm
REFLECTION
μ = 10⁻⁴ cm⁻¹
(η = 8′)
μ = 0·45 cm⁻¹
(η = 8′)
▲ EXPERIMENTAL
○ B & L MODEL
(η = 6′)
△ B & L MODEL
(η = 8′)
PEAK REFLECTIVITY
WAVELENGTH (Å)
1·0
0·8
0·6
0·4
0·2
0
0·5
1·0
1·5
2·0
2·5

Fig. IV-6

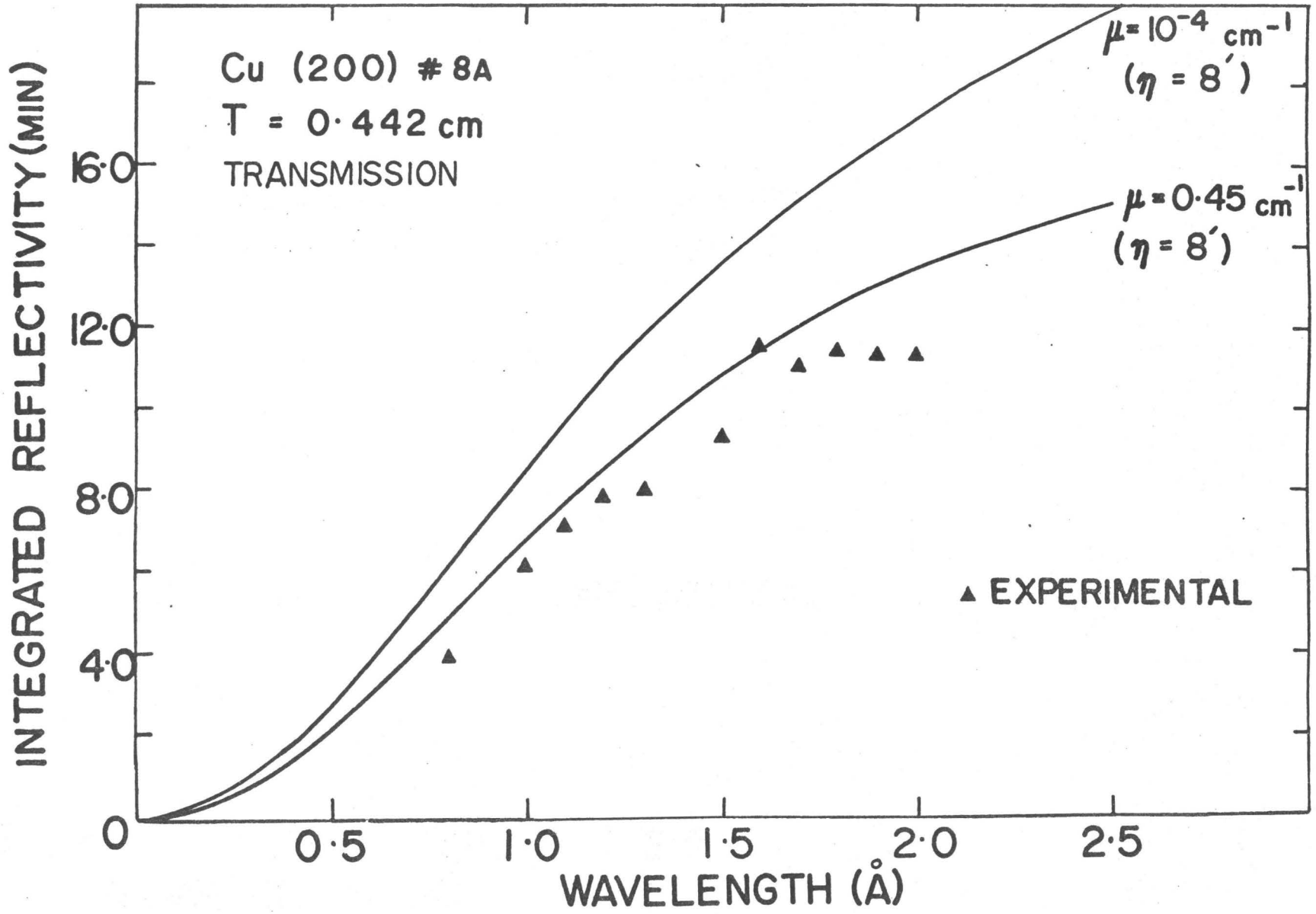
Cu (200) # 8A
T = 0·442 cm
TRANSMISSION
μ = 10⁻⁴ cm⁻¹
(η = 8′)
μ = 0·45 cm⁻¹
(η = 8′)
▲ EXPERIMENTAL
INTEGRATED REFLECTIVITY (MIN)
16·0
12·0
8·0
4·0
0
0·5
1·0
1·5
2·0
2·5
WAVELENGTH (Å)

Fig. IV-7

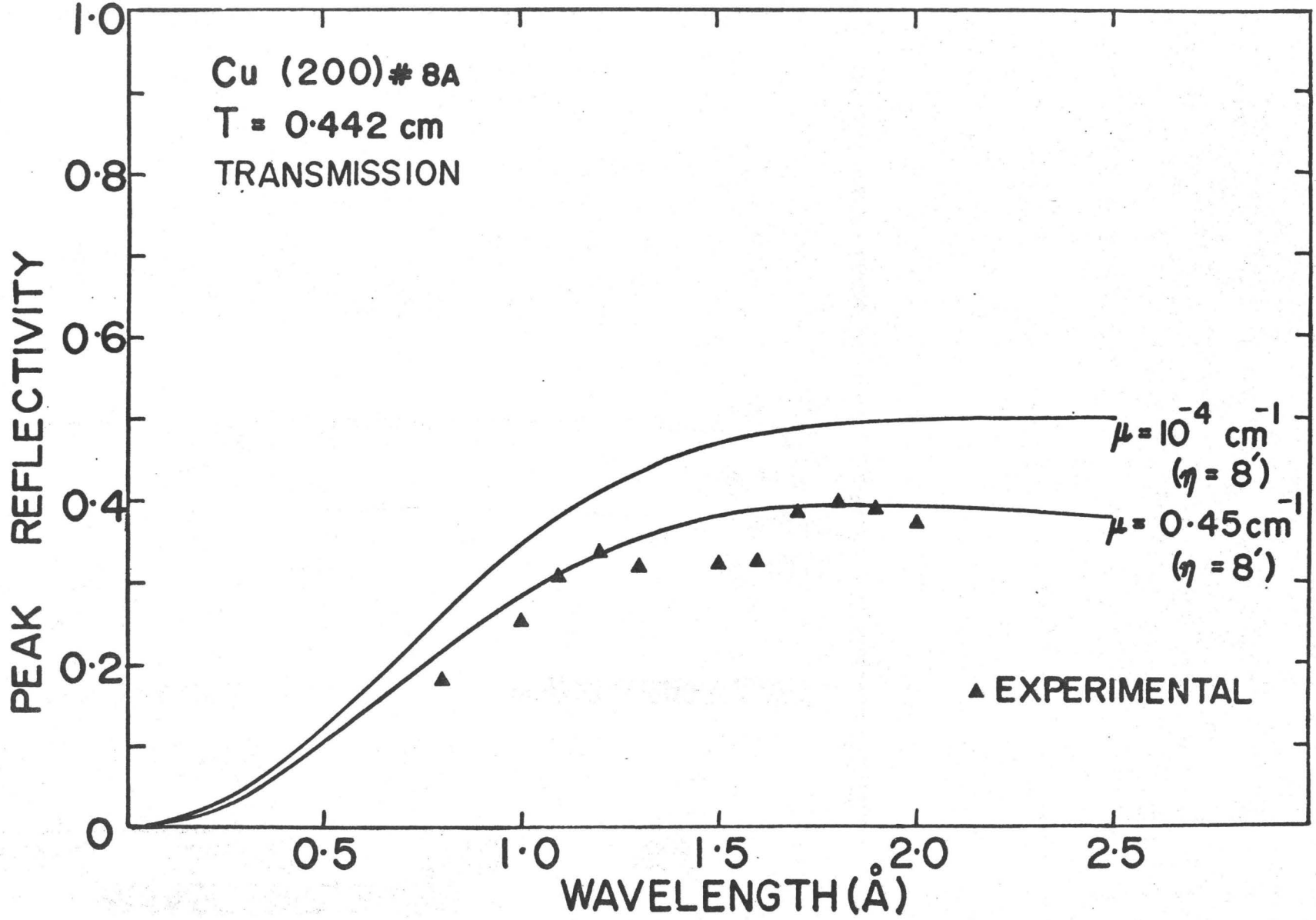
Cu (200) # 8A
T = 0·442 cm
TRANSMISSION
PEAK REFLECTIVITY
1·0
0·8
0·6
0·4
0·2
0
0·5
1·0
1·5
2·0
2·5
WAVELENGTH (Å)
μ = 10⁻⁴ cm⁻¹
(η = 8′)
μ = 0·45 cm⁻¹
(η = 8′)
▲ EXPERIMENTAL

Fig. IV-8

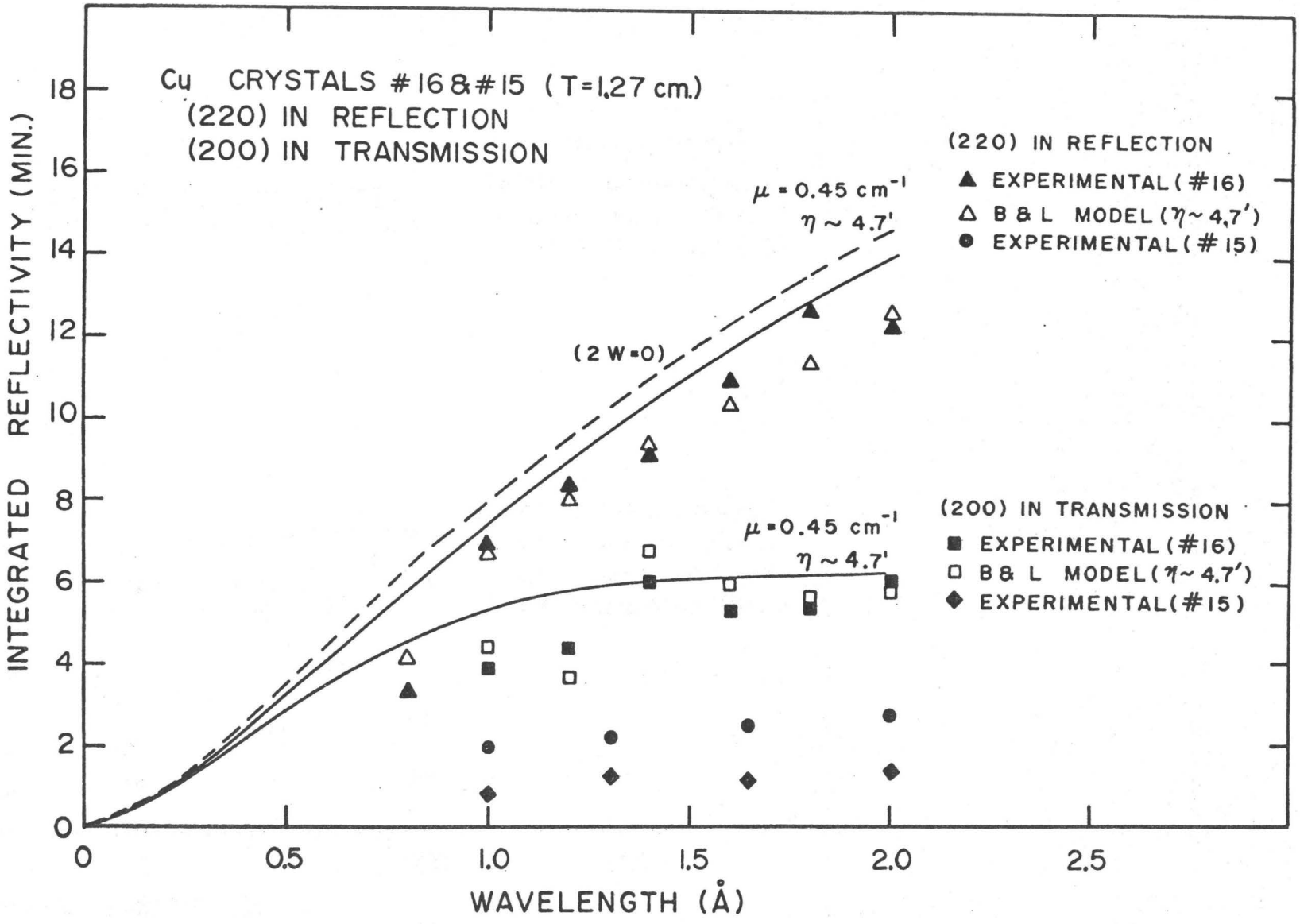
Cu CRYSTALS #16 & #15 (T=1.27 cm.)
(220) IN REFLECTION
(200) IN TRANSMISSION
(220) IN REFLECTION
▲ EXPERIMENTAL (#16)
△ B & L MODEL (η~4.7')
● EXPERIMENTAL (#15)
μ = 0.45 cm⁻¹
η ~ 4.7'
(2W=0)
μ = 0.45 cm⁻¹
η ~ 4.7'
(200) IN TRANSMISSION
■ EXPERIMENTAL (#16)
□ B & L MODEL (η~4.7')
◆ EXPERIMENTAL (#15)
INTEGRATED REFLECTIVITY (MIN.)
WAVELENGTH (Å)
0
2
4
6
8
10
12
14
16
18
0
0.5
1.0
1.5
2.0
2.5

Fig. IV-9

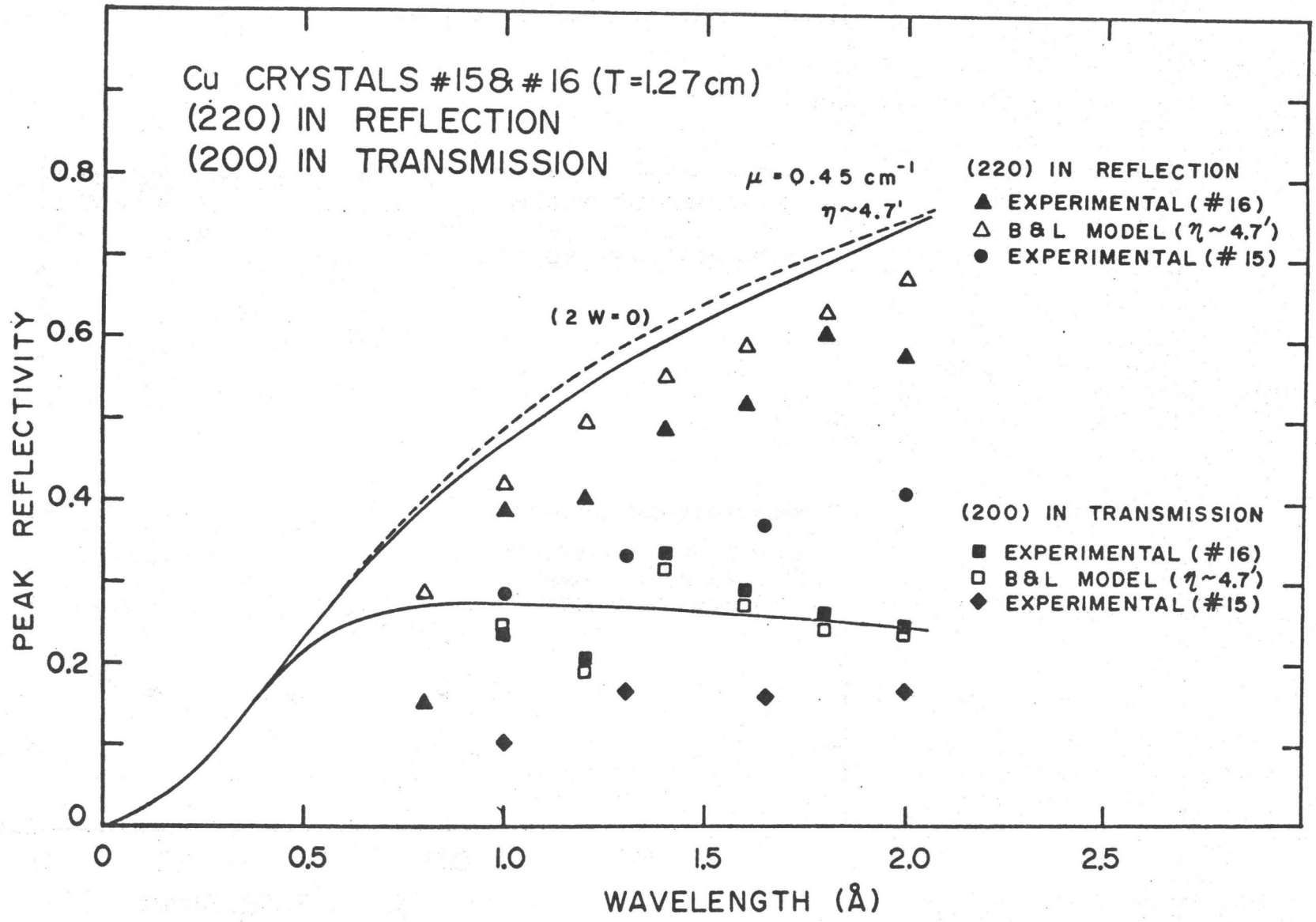
Cu CRYSTALS #15 & #16 (T=1.27cm)
(220) IN REFLECTION
(200) IN TRANSMISSION
μ = 0.45 cm⁻¹
η~4.7'
(2W=0)
(220) IN REFLECTION
▲ EXPERIMENTAL (#16)
△ B&L MODEL (η~4.7')
● EXPERIMENTAL (#15)
(200) IN TRANSMISSION
■ EXPERIMENTAL (#16)
□ B&L MODEL (η~4.7')
◆ EXPERIMENTAL (#15)
PEAK REFLECTIVITY
0
0.2
0.4
0.6
0.8
0
0.5
1.0
1.5
2.0
2.5
WAVELENGTH (Å)

Fig. IV-10

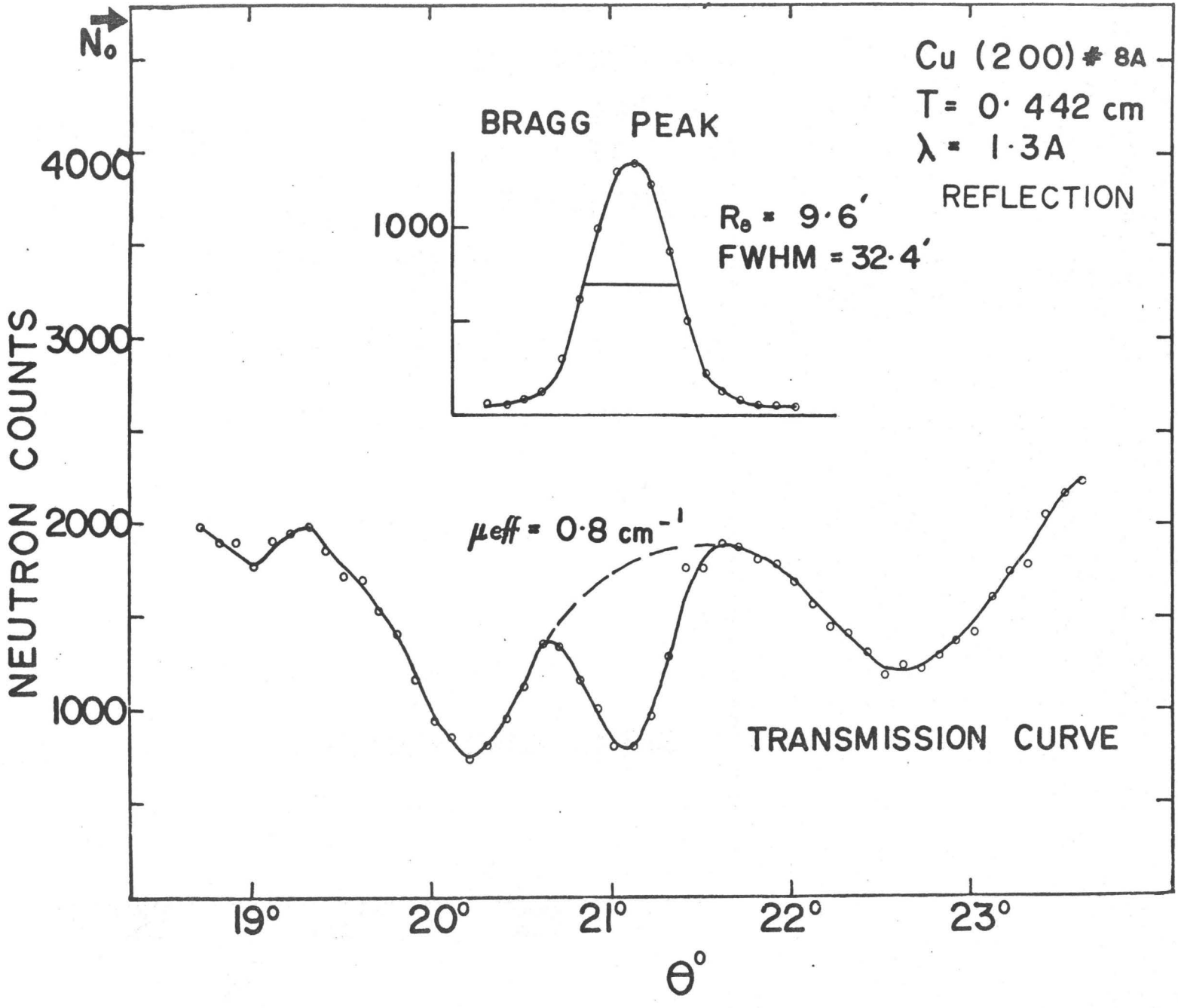

Fig. IV-11 Typical experimental results used to calculate R_θ for λ = 1.3 Å and T = 0.442 cm for crystal #8A. The three dips in the transmission curve exhibit the presence of simultaneous reflections.

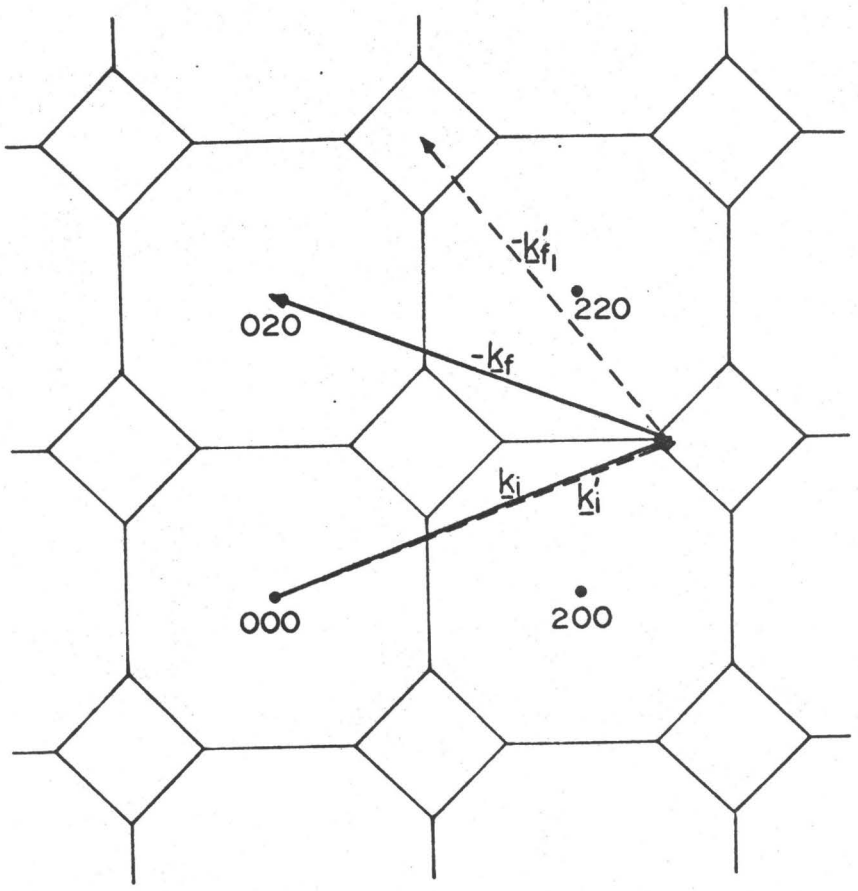
-Kf1
220
020
-Kf
Ki
Ki'
000
200

(a)

Fig. IV-12

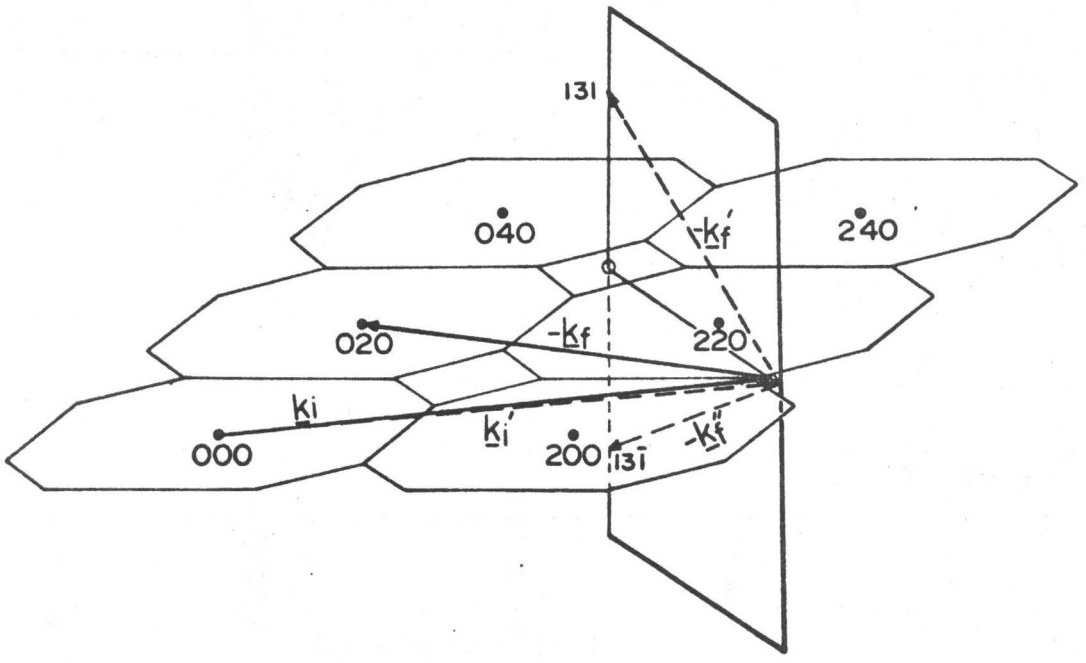
131
040
-Kf'
240
020
-Kf
220
Ki
000
Ki'
200
131̄
-Kf''

(b)

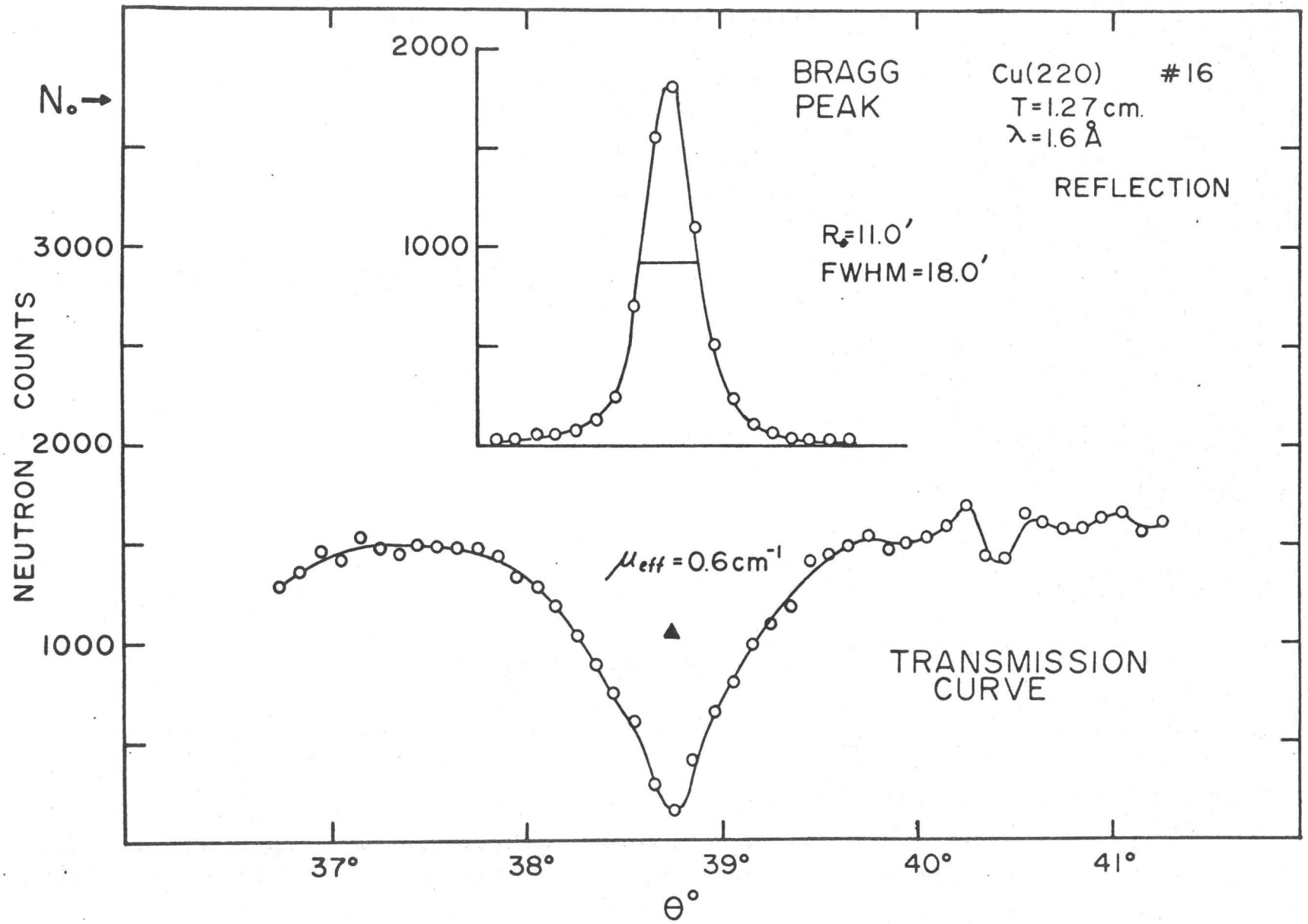

Fig. IV-13 Typical experimental results used to calculate R_θ for λ = 1.6 Å and T = 1.27 cm for crystal #16.

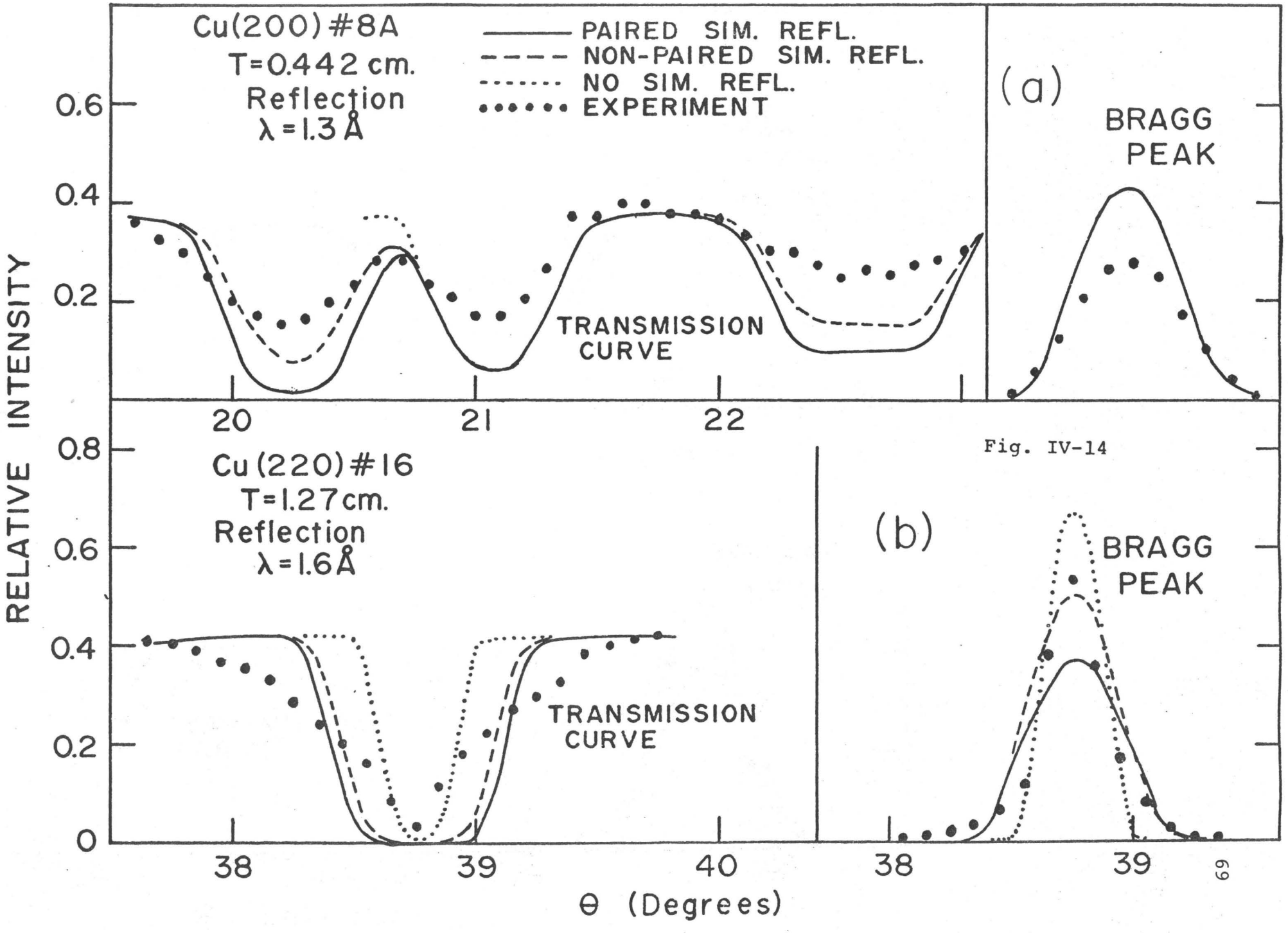
Cu(200)#8A
T=0.442 cm.
Reflection
λ=1.3 Å
PAIRED SIM. REFL.
NON-PAIRED SIM. REFL.
NO SIM. REFL.
EXPERIMENT
(a)
BRAGG PEAK
TRANSMISSION CURVE
Cu(220)#16
T=1.27cm.
Reflection
λ=1.6Å
(b)
BRAGG PEAK
TRANSMISSION CURVE
RELATIVE INTENSITY
Θ (Degrees)
0
0.2
0.4
0.6
0.8
20
21
22
38
39
40

Fig. IV-14

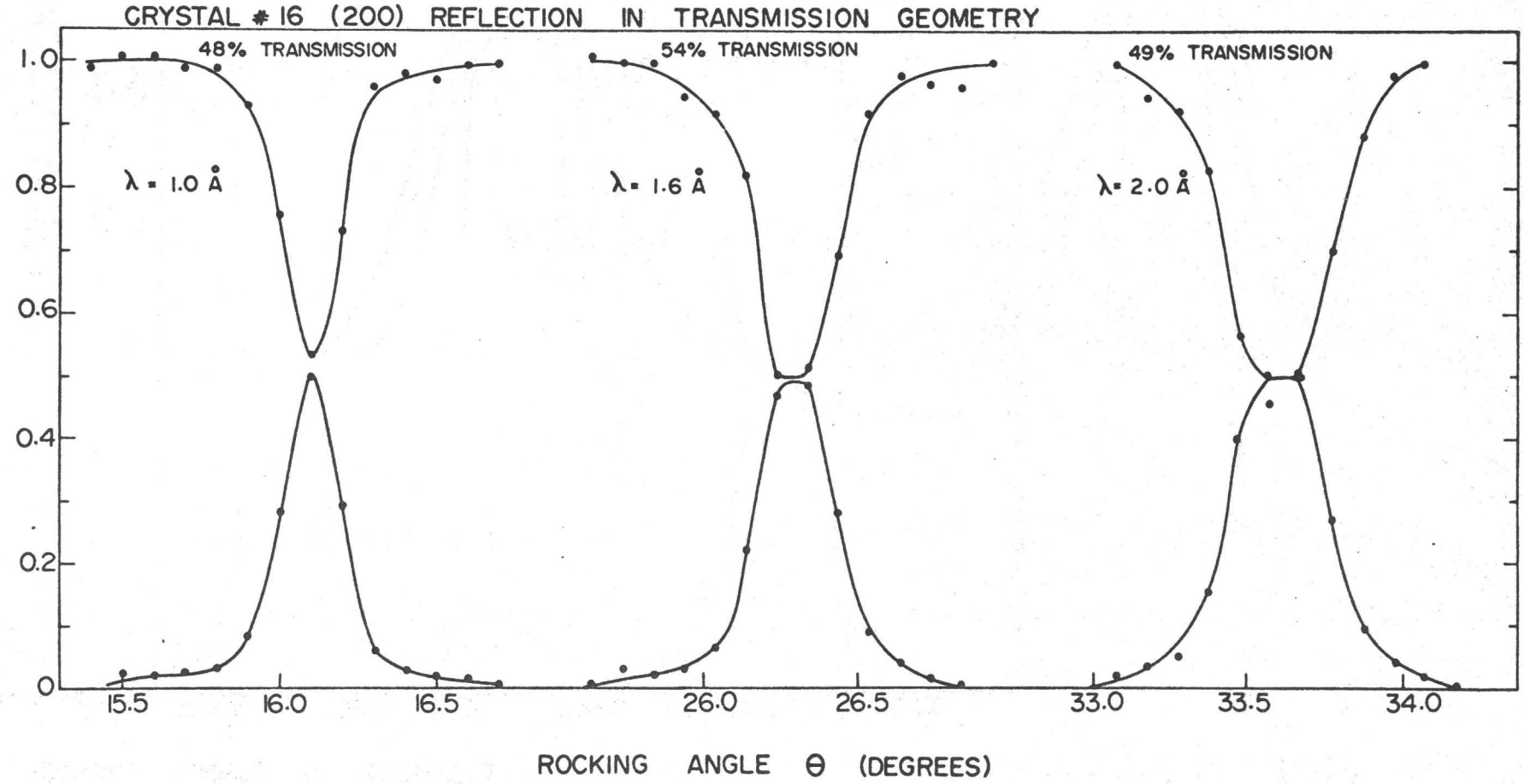

Fig. IV-15 A plot for crystal #16, showing the mirror images of the Bragg peak and transmission curves obtained in transmission geometry.

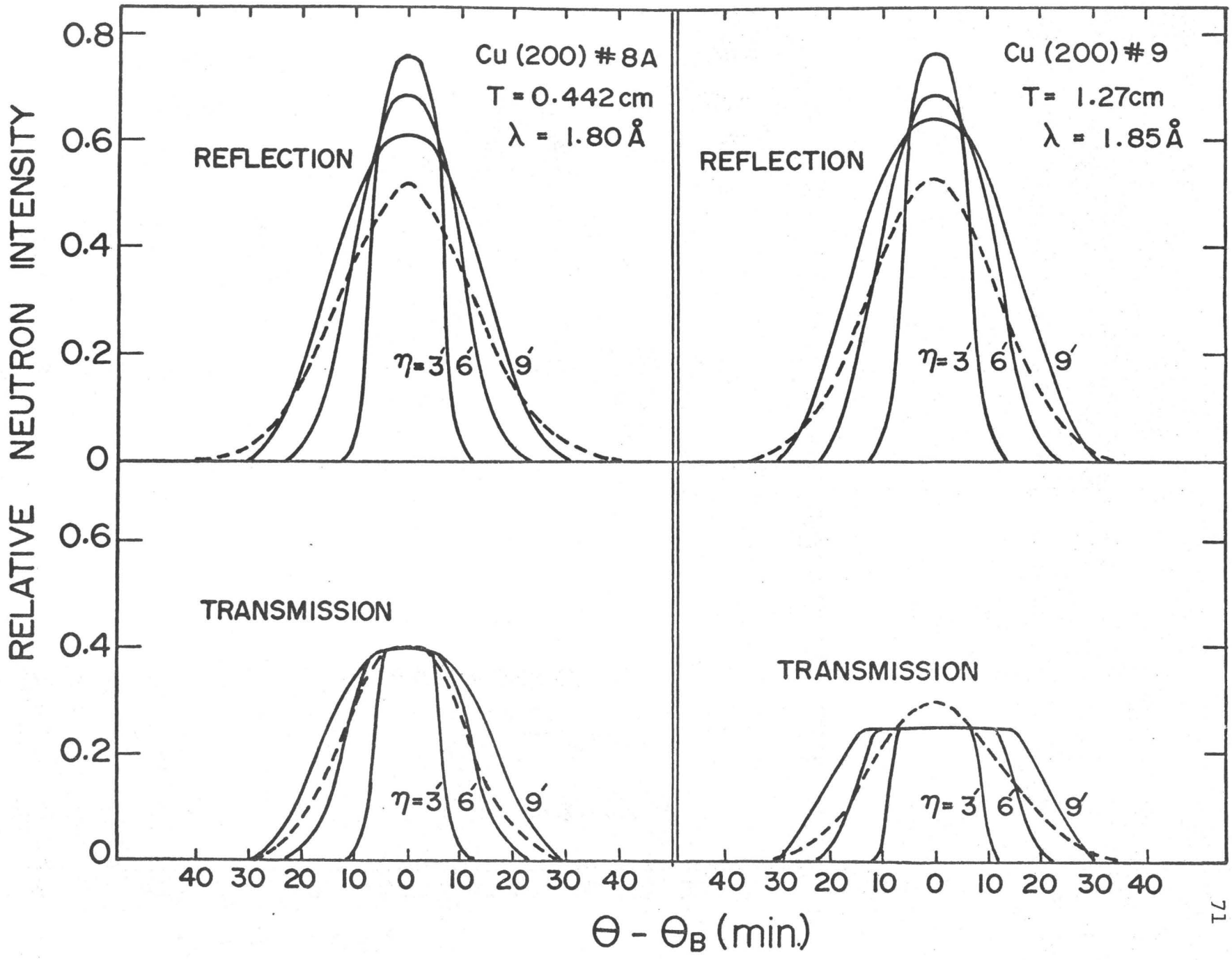
RELATIVE NEUTRON INTENSITY
0.8
0.6
0.4
0.2
0
Cu (200) # 8A
T = 0.442 cm
λ = 1.80 Å
REFLECTION
η=3′ 6′ 9′
Cu (200) # 9
T = 1.27cm
λ = 1.85 Å
REFLECTION
η=3′ 6′ 9′
TRANSMISSION
η=3′ 6′ 9′
TRANSMISSION
η=3′ 6′ 9′
40 30 20 10 0 10 20 30 40
40 30 20 10 0 10 20 30 40
Θ - Θ_B (min.)

Fig. IV-16

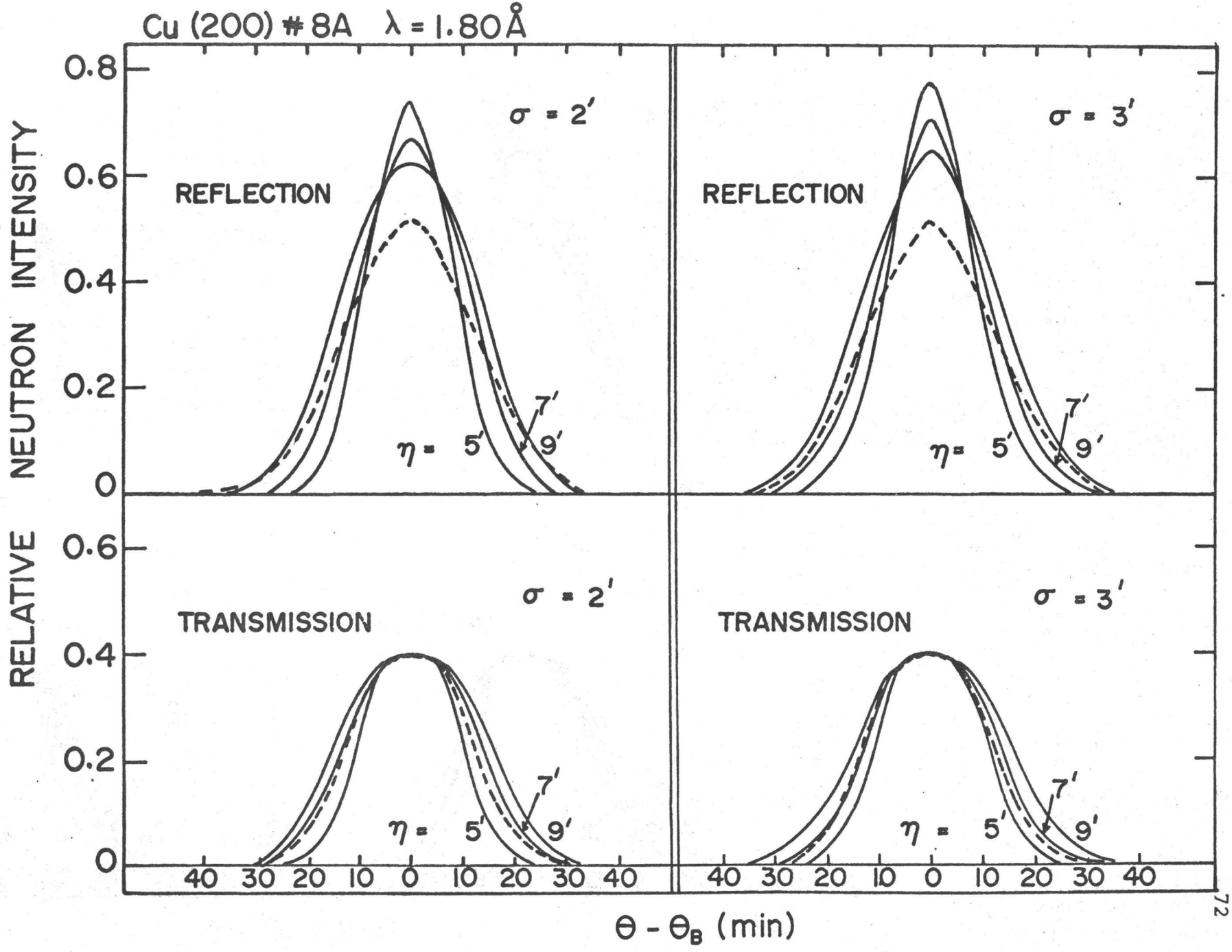
Cu (200) # 8A λ = 1.80 Å
RELATIVE NEUTRON INTENSITY
0.8
0.6
0.4
0.2
0
REFLECTION
σ = 2′
η = 5′
7′
9′
REFLECTION
σ = 3′
η = 5′
7′
9′
TRANSMISSION
σ = 2′
η = 5′
7′
9′
TRANSMISSION
σ = 3′
η = 5′
7′
9′
40 30 20 10 0 10 20 30 40
Θ - Θ_B (min)

Fig. IV-17

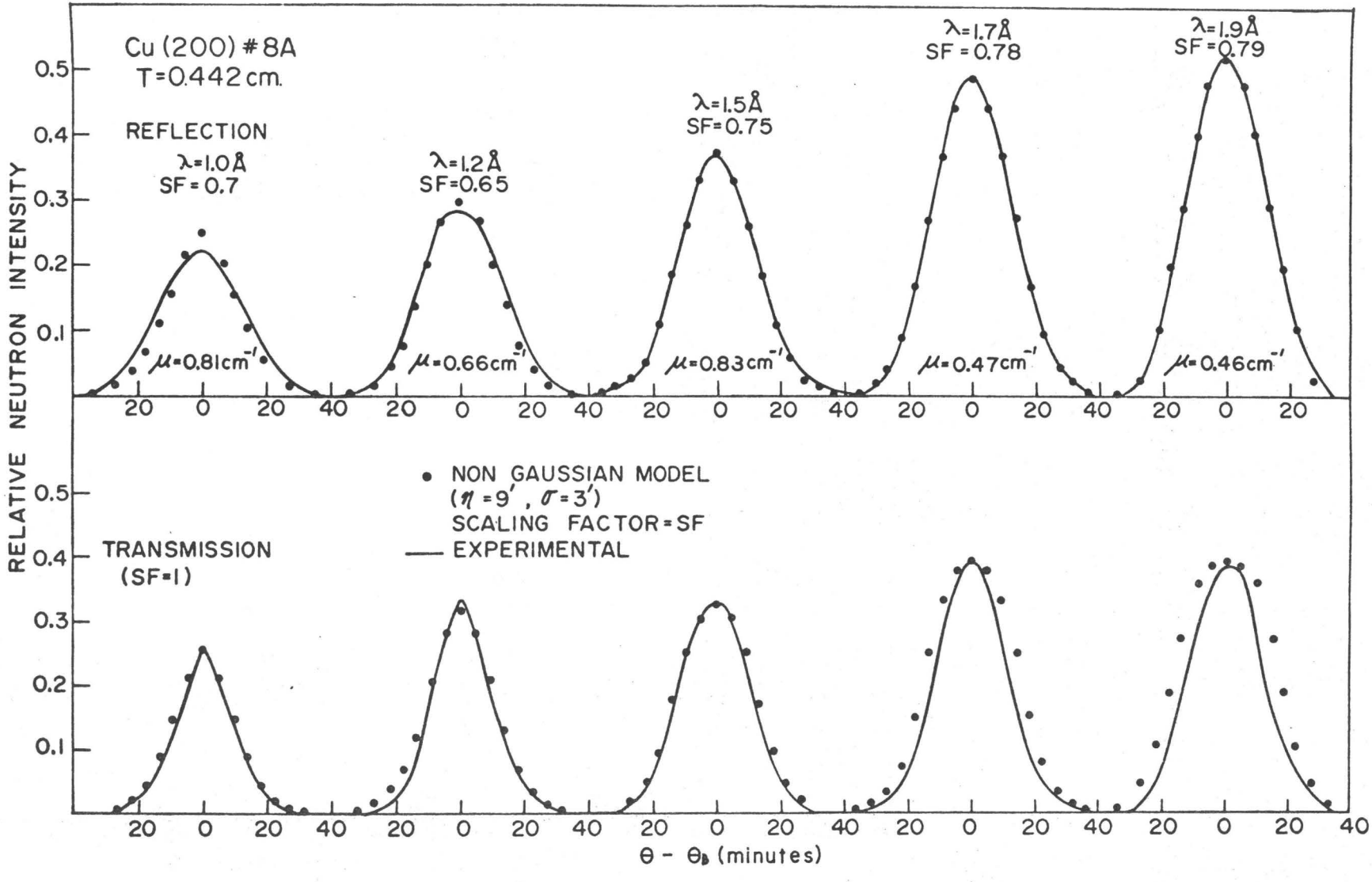

Fig. IV-18 Comparison of Bragg peak shapes for crystal # 8A, Cu(200), at several values of λ, using the non Gaussian B & L model and a scale factor applied directly to the peak intensity.

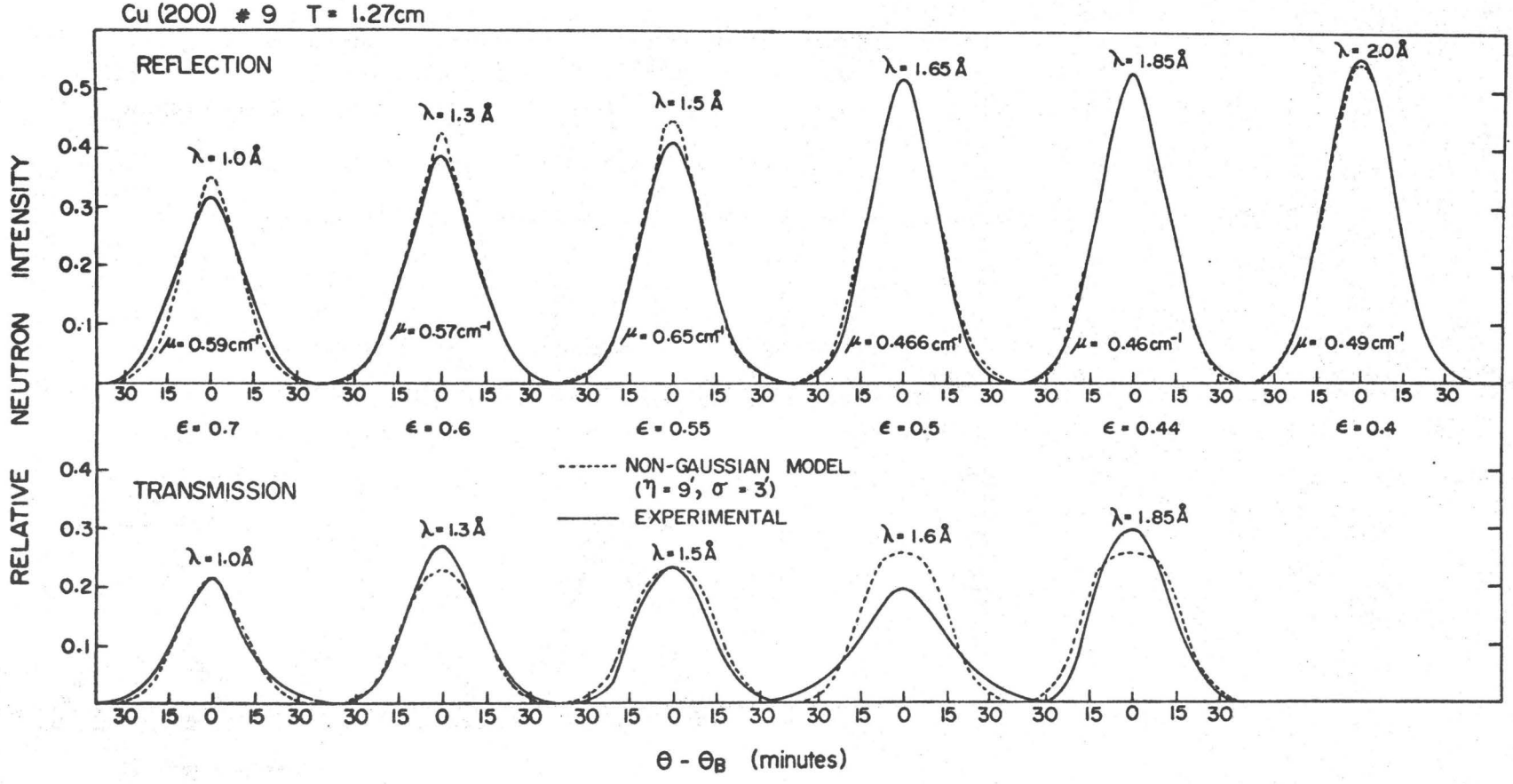

Fig. IV-19 Comparison of Bragg peak shapes for crystal #9, Cu(200), at several values of λ, using the non Gaussian B & L model and a Q which has been scaled by ε.

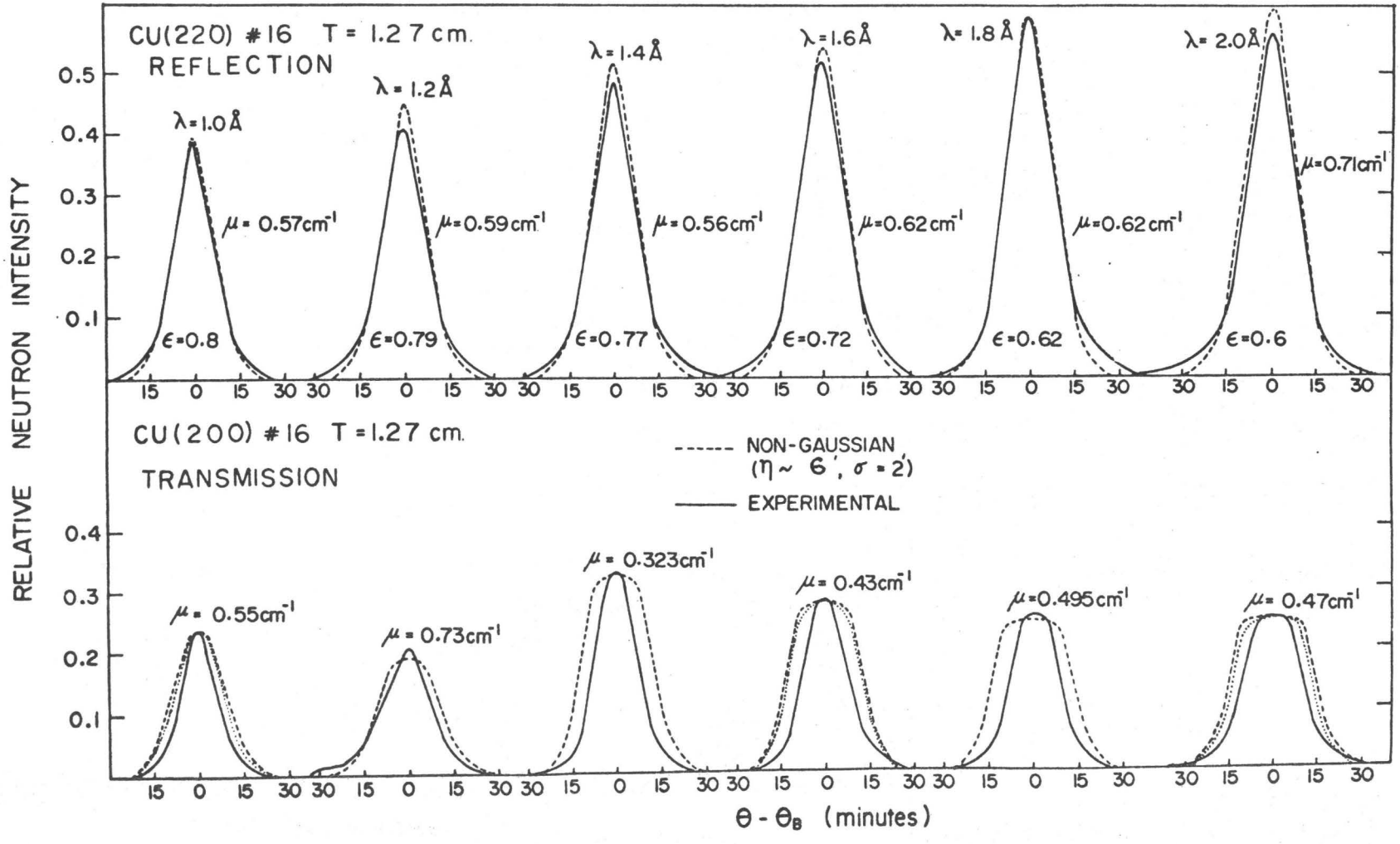

Fig. IV-20 Comparison of Bragg peak shapes for crystal #16, Cu(220), at several values of λ, using the non Gaussian B & L model and a Q which has been scaled by ε.

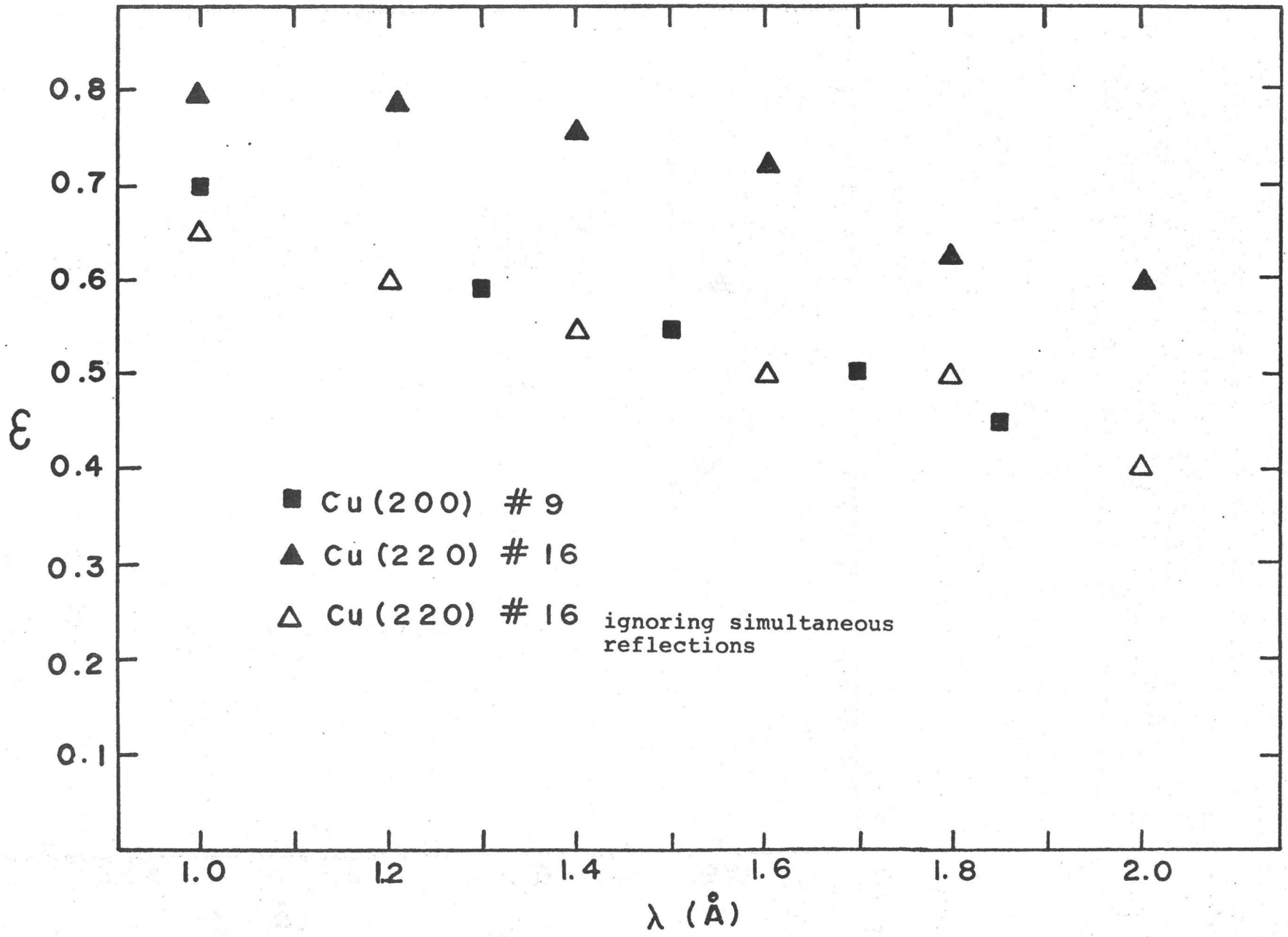

Fig. IV-21 Experimental relationship between ε and λ for crystals #9, Cu(200), and #16, Cu(220).

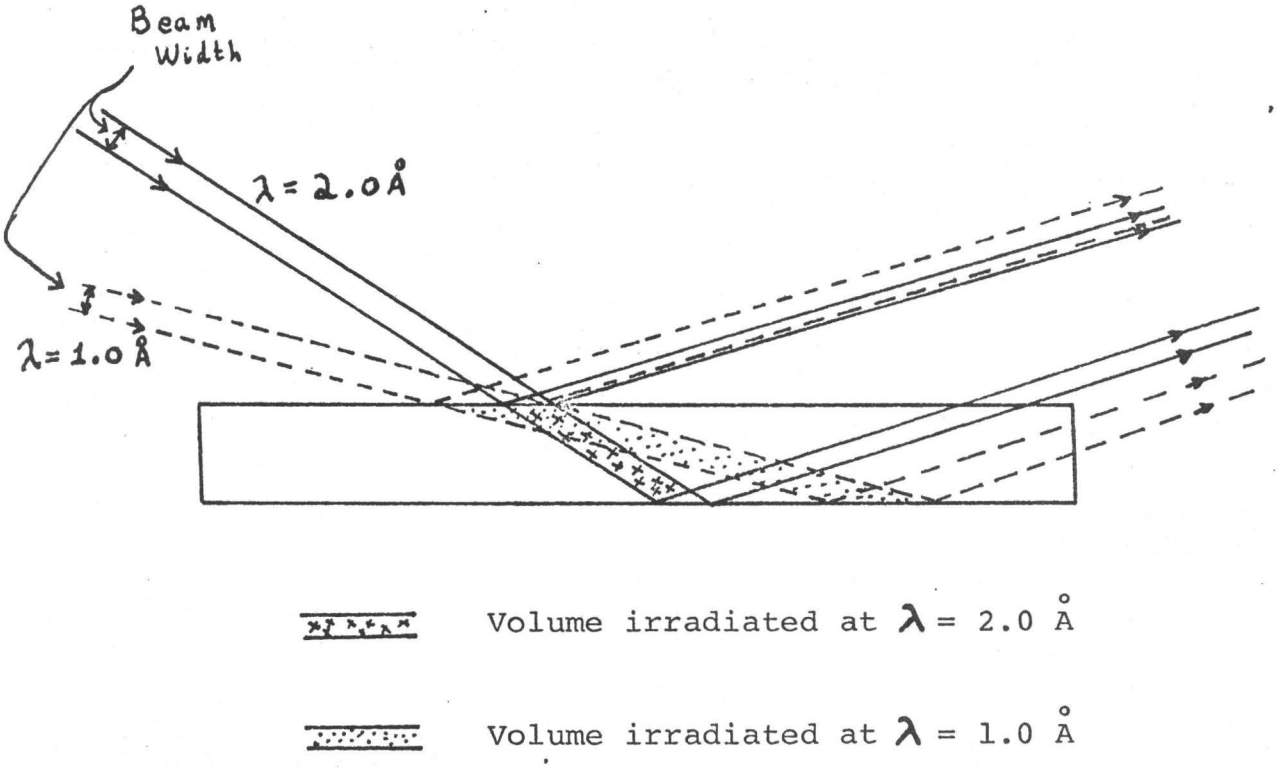

Fig. IV-22 Diagram showing the dependance on wavelength of the volume of crystal irradiated.

APPENDIX I

Normalization of the Non-Gaussian Mosaic Block Distribution

The unnormalized mosaic distribution function is given by

$$W(\Delta) = \frac{1}{\sqrt{2\pi}} \int_0^\infty \frac{1}{\eta} e^{-\frac{\Delta^2}{2\eta^2}} e^{-(\eta-\eta_o)^2/2\sigma^2} \, d\eta$$

Thus, to normalize $W(\Delta)$, we require that

$$N = \int_{-\infty}^{\infty} W(\Delta) d\Delta = 1$$

where N is the appropriate normalization factor. Substituting the first equation into the second, one obtains

$$N \int_{-\infty}^{\infty} \int_0^\infty \frac{1}{\sqrt{2\pi}\eta} e^{-\Delta^2/2\eta^2} e^{-(\eta-\eta_o)^2/2\sigma^2} \, d\eta d\Delta = 1$$

Integrating over Δ yields

$$N = \int_0^\infty e^{-(\eta-\eta_o)^2/2\sigma^2} \, d\eta = 1$$

Letting $\eta-\eta_o = \xi$, the last equation becomes

$$N = 1/[\int_{-\eta_o}^{0} e^{-\xi^2/2\sigma^2} \, d\xi + \int_0^\infty e^{-\xi^2/2\sigma^2} \, d\xi]$$

$$= 1/[\int_{-\eta_o}^{0} e^{-\xi^2/2\sigma^2} \, d\xi + \frac{\sqrt{2\pi}}{2}\sigma]$$

and thus the normalized mosaic distribution function becomes

$$W(\Delta) = \frac{\int_{o}^{\infty} \frac{1}{\eta} e^{-\frac{\Delta^2}{2\eta^2}} e^{-(\eta-\eta_o)^2/2\sigma^2} d\eta}{\sqrt{2\pi} \int_{-\eta_o}^{o} e^{-\xi^2/2\sigma^2} d\xi + \pi\sigma}$$

QED.

APPENDIX II

Power Equations with Paired Simultaneous Reflections

The set of equations II-6, are written out in full for two simultaneous reflections, below.

$$\frac{dP_1}{dt} = -\frac{P_1}{\gamma_1}(\mu + R_{12} + R_{13} + R_{14}) + \frac{P_2}{\gamma_2} R_{21} + \frac{P_3}{\gamma_3} R_{31} + \frac{P_4}{\gamma_4} R_{41}$$

$$\pm \frac{dP_2}{dt} = \frac{P_1}{\gamma_1} R_{12} - \frac{P_2}{\gamma_2}(\mu + R_{21} + R_{23} + R_{24}) + \frac{P_3}{\gamma_3} R_{32} + \frac{P_4}{\gamma_4} R_{42}$$

$$\pm \frac{dP_3}{dt} = \frac{P_1}{\gamma_1} R_{13} + \frac{P_2}{\gamma_2} R_{23} - \frac{P_3}{\gamma_3}(\mu + R_{31} + R_{32} + R_{34}) + \frac{P_4}{\gamma_4} R_{43}$$

$$\pm \frac{dP_4}{dt} = \frac{P_1}{\gamma_1} R_{14} + \frac{P_2}{\gamma_2} R_{24} + \frac{P_3}{\gamma_3} R_{34} - \frac{P_4}{\gamma_4}(\mu + R_{41} + R_{42} + R_{43})$$

If the simultaneous reflections designated by powers P_3 and P_4 are paired, then by symmetry $R_{13}=R_{14}$, $R_{23}=R_{24}$, $P_3(t)=P_4(t)$, and $\gamma_3=\gamma_4$. Therefore, the above equations can be reduced by substitution to the following set of differential equations.

$$\frac{dP_1}{dt} = \frac{-P_1}{\gamma_1}(\mu + R_{12} + 2R_{13}) + \frac{P_2}{\gamma_2} R_{21} + 2\frac{P_3}{\gamma_3} R_{31}$$

$$\pm \frac{dP_2}{dt} = \frac{P_1}{\gamma_1} R_{12} - \frac{P_2}{\gamma_2}(\mu + R_{21} + 2R_{23}) + 2\frac{P_3}{\gamma_3} R_{32}$$

$$\pm \frac{dP_3}{dt} = \frac{P_1}{\gamma_1} R_{13} + \frac{P_2}{\gamma_2} R_{23} - \frac{P_3}{\gamma_3}(\mu + R_{31} + R_{32})$$

$$\pm \frac{dP_4}{dt} = \frac{P_1}{\gamma_1} R_{13} + \frac{P_2}{\gamma_2} R_{23} - \frac{P_3}{\gamma_3}(\mu + R_{31} + R_{32})$$

Since the latter two equations are the same, one need only solve the set of three differential equations and hence the pairing of simultaneous reflections is accounted for by replacing R_{13} and R_{23} by $2R_{13}$ and $2R_{23}$ respectively, in the first two equations only.

QED

APPENDIX III

Effect of Parallelism on Measured Peak Widths

Let us consider the case of a reflecting system composed of two crystals with lattice spacings d_1 and d_2 as shown in the accompanying figure. In tracing the path of the neutrons which pass through the centre of collimator C_1, one finds that the Bragg condition must be satisfied twice such that

$$\lambda = 2d_1\sin\theta_1 = 2d_2\sin\theta_2$$

where θ_1 and θ_2 are the angles of incidence of the neutron beam of wavelength λ on crystals 1 and 2 respectively.

If the angular divergence of C_1 is $\Delta\theta_1$, then the extreme value of wavelength which will be reflected from crystal 1 is defined by $\lambda' = 2d_1\sin(\theta_1 + \Delta\theta_1)$ and hence reflection of the same beam from crystal 2 must obey

$$\lambda' = 2d_2\sin(\theta_2 + \Delta\theta_1 + \Delta\theta_2).$$

Hence, $\lambda' = 2d_1(\sin\theta_1\cos\Delta\theta_1 + \cos\theta_1\sin\Delta\theta_1)$

$$= 2d_2[\sin\theta_2\cos(\Delta\theta_1 + \Delta\theta_2) + \cos\theta_2\sin(\Delta\theta_1 + \Delta\theta_2)]$$

Thus, in the approximation that $\Delta\theta_1$ and $\Delta\theta_2$ are each small, compared to θ_1 and θ_2, one finds

$$\lambda' = 2d_1(\sin\theta_1 + \Delta\theta_1\cos\theta_1)$$

$$= 2d_2(\sin\theta_2 + (\Delta\theta_1 + \Delta\theta_2)\cos\theta_2)$$

Substituting and solving for $\Delta\theta_2$, one finds,

$$\Delta\theta_2 = \Delta\theta_1 \left[\frac{\tan\theta_2}{\tan\theta_1} - 1 \right]$$

Thus, the broadening of the measured peaks arising from geometrical factors is given by $\Delta\theta_2$ and the measured width is obtained from the quantity

$$[\eta_1^2 + \eta_2^2 + \Delta\theta_2^2]^{1/2}$$

where η_1 and η_2 are the mosaic distribution parameters of the first and second crystals respectively.

Thus, it becomes clear that the contribution to the measured width due to parallelism becomes negligeable as $\theta_1 \rightarrow \theta_2$. If also the monochromator width, η_1, is very small, then the measured width thus becomes η_2, the true width of the sample crystal.

By applying the above information to the experiments discussed in Chapter III, one finds $\eta_1 \approx 0$ for Ge, $\Delta\theta_1 = 0.0125$ and $\Delta\theta_2$ can be calculated for each value of λ. Table A.3.1 indicates values of $\Delta\theta_2$ at three different values of λ. From this table, it is clear that a degree of parallelism has been attained such that the widths obtained from experiment are due, to all intensive purposes, to the width of the sample crystal itself.

TABLE A.3.1 Contributions to the measured FWHM due to non-parallelism for crystal #16.

Cu(220) #16

λ (Å)	θ_1 (Ge)	θ_2 (Cu)	$\Delta\theta_2$	FWHM (measured)	η_2
1.0	22.7°	23.1°	0.86'	16'	16'
1.6	38.1°	38.8°	1.1'	18'	18'
2.0	50.2°	51.5°	2.2'	18'	17.9'

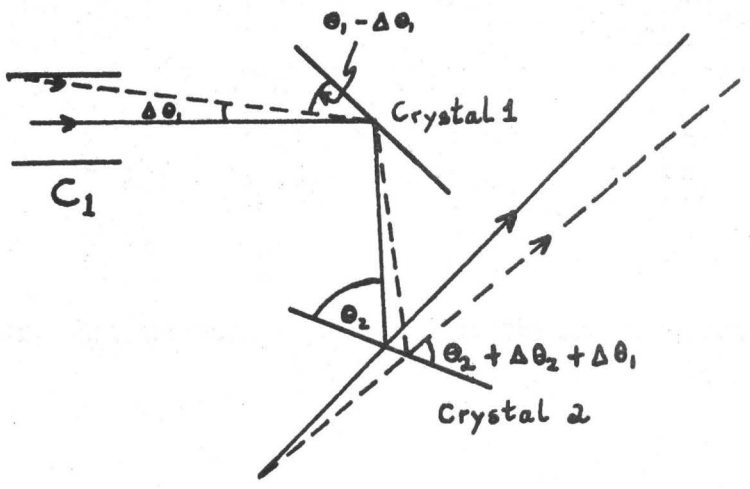

Fig. A.3.1 The effect of parallelism on reflection from two crystals.

BIBLIOGRAPHY

Arndt, U.W., Willis, B.T.M., Single Crystal Diffractometry, Cambridge University Press (1966).

Bacon, G.E., Neutron Diffraction, 2nd Edition. Oxford University Press (1962).

Bacon, G.E. and Lowde, R.D., Acta Cryst. 1, 303 (1948).

Blinowski, K. and Sosnowski, J., Nuclear Instruments and Methods 10, 289 (1961).

Borgonovi, G. and Caglioti, G., Nuovo Cimento 24, 1174 (1962).

Brockhouse, B.N., Nuovo Cimento, Suppl. 9, 45 (1958).

Brockhouse, B.N., deWit, G.A., Hallman, E.D. and Rowe, J.M., Neutron Inelastic Scattering, Vol. 2 (IAEA, Vienna) 259 (1968).

Brogren, G., Acta Cryst. A25, 111 (1969).

Brugger, R.M., Thermal Neutron Scattering, edited by P.A. Egelstaff, Academic Press Inc., N.Y., 53 (1965).

Burbank, R.D., Acta Cryst. 17, 434 (1964).

Caglioti, G., Acta Cryst. 17, 1202 (1964).

Darwin, C.G., Phil. Mag. 27, 315 and 675 (1914).

DeMarco, J.J. and Weiss, R.J., Acta Cryst. 15, 1125 (1962).

Dorner, B., to be published (1970).

Dymond, R.R. and Brockhouse, B.N., to be published in Proceedings of Panel on Instrumentation for Neutron Inelastic Scattering Research, IAEA, Vienna (1970).

Egelstaff, P.A., Thermal Neutron Scattering, Academic Press Inc. N.Y. (1965).

Gay, P., Hirsch, P.B. and Kelly, A., Acta Metallurgica 1, 315 (1953).

Hallman, E.D., Ph.D. thesis (1969).

James, R.W., The Optical Principles of the Diffraction of X-rays, G. Bell and Sons Ltd. London (1948).

Larson, J.A. and Corey, C.L., J. App. Phys. 40, 2708 (1969).

Moon, R.M. and Shull, C.G., Acta Cryst. 17, 805 (1964).

O'Connor, D.A. and Sosnowski, J., Acta Cryst. 14, 292 (1961).

Popovici, M., Gheorghiu, Z. and Gelberg, D., Nuclear Instruments and Methods 69, 125 (1969).

Renninger, M., Z. Phys. 106, 141 (1937).

Roy, A.P., private communication (1970).

Turberfield, K.C., AERE-R 5647, Harwell (1968).

Willis, B.T.M., Proc. R. Soc. A, 274, 122 (1963).

Zachariasen, W.H., Theory of X-ray Diffraction in Crystals, J. Wiley and Sons, Inc. (1945).